Atmos. Chem. Phys., 16, 3609–3629, 2016
www.atmos-chem-phys.net/16/3609/2016/
doi:10.5194/acp-16-3609-2016

Atmospheric Chemistry and Physics Open Access EGU

Trapping, chemistry, and export of trace gases in the South Asian summer monsoon observed during CARIBIC flights in 2008

Armin Rauthe-Schöch[1], Angela K. Baker[1], Tanja J. Schuck[1,a], Carl A. M. Brenninkmeijer[1], Andreas Zahn[2], Markus Hermann[3], Greta Stratmann[4], Helmut Ziereis[4], Peter F. J. van Velthoven[5], and Jos Lelieveld[1]

[1]Max Planck Institute for Chemistry (Otto Hahn Institute), Department of Atmospheric Chemistry, Mainz, Germany
[2]Karlsruhe Institute of Technology (KIT), Institute for Meteorology and Climate Research, Karlsruhe, Germany
[3]Leibniz Institute for Tropospheric Research (TROPOS), Leipzig, Germany
[4]German Aerospace Center (DLR), Institute for Atmospheric Physics, Oberpfaffenhofen, Germany
[5]Royal Netherlands Meteorological Institute (KNMI), De Bilt, the Netherlands
[a]now at: Goethe University Frankfurt, Institute for Atmospheric and Environmental Sciences, Frankfurt am Main, Germany

Correspondence to: Armin Rauthe-Schöch (armin.rauthe-schoech@mpic.de)

Received: 6 February 2015 – Published in Atmos. Chem. Phys. Discuss.: 10 March 2015
Revised: 22 February 2016 – Accepted: 1 March 2016 – Published: 17 March 2016

Abstract. The CARIBIC (Civil Aircraft for the Regular Investigation of the Atmosphere Based on an Instrument Container) passenger aircraft observatory performed in situ measurements at 10–12 km altitude in the South Asian summer monsoon anticyclone between June and September 2008. These measurements enable us to investigate this atmospheric region (which so far has mostly been observed from satellites) using the broad suite of trace gases and aerosol particles measured by CARIBIC. Elevated levels of a variety of atmospheric pollutants (e.g. carbon monoxide, total reactive nitrogen oxides, aerosol particles, and several volatile organic compounds) were recorded. The measurements provide detailed information about the chemical composition of air in different parts of the monsoon anticyclone, particularly of ozone precursors. While covering a range of 3500 km inside the monsoon anticyclone, CARIBIC observations show remarkable consistency, i.e. with distinct latitudinal patterns of trace gases during the entire monsoon period.

Using the CARIBIC trace gas and aerosol particle measurements in combination with the Lagrangian particle dispersion model FLEXPART, we investigated the characteristics of monsoon outflow and the chemical evolution of air masses during transport. The trajectory calculations indicate that these air masses originated mainly from South Asia and mainland Southeast Asia. Estimated photochemical ages of the air were found to agree well with transport times from a source region east of 90–95° E. The photochemical ages of the air in the southern part of the monsoon anticyclone were systematically younger (less than 7 days) and the air masses were mostly in an ozone-forming chemical mode. In its northern part the air masses were older (up to 13 days) and had unclear ozone formation or destruction potential. Based on analysis of forward trajectories, several receptor regions were identified. In addition to predominantly westward transport, we found evidence for efficient transport (within 10 days) to the Pacific and North America, particularly during June and September, and also of cross-tropopause exchange, which was strongest during June and July. Westward transport to Africa and further to the Mediterranean was the main pathway during July.

1 Introduction

During boreal summer the South Asian monsoon dominates atmospheric circulation over Asia, and has a strong influence on atmospheric transport and chemistry of much of the Northern Hemisphere (Randel and Jensen, 2013). The monsoon is characterised by a persistent large-scale anticyclonic structure in the upper troposphere, centred over Pakistan and northern India, framed by the subtropical eastward jet in the north and a westward equatorial jet in the south. This upper troposphere anticyclone (UTAC) is not static but oscillates in strength, shape, and position (Garny and Randel, 2013).

At the same time it features a strikingly distinct composition signature throughout the monsoon season. Observations from satellites have shown an enhancement of mixing ratios of a number of trace gases in the UTAC, most prominently methane (CH_4) (Xiong et al., 2009) and carbon monoxide (CO) (Kar et al., 2004). Since the monsoon is accompanied by strong convection, upper tropospheric trace gas mixing ratios are directly linked to surface emissions in this densely populated region. In addition, polluted air masses can be trapped and accumulate inside the UTAC, where they can be chemically isolated for several days (Randel and Park, 2006; Park et al., 2008). The UTAC can also play a governing role in the dispersion of volcanic plumes, e.g. after the June 2011 eruption of the Nabro volcano in Eritrea (Fairlie et al., 2014). Outflow occurs predominantly westward towards northern Africa and the Middle East, where a summertime ozone (O_3) maximum due to ozone formation in monsoon outflow has been reported (Li et al., 2001; Liu et al., 2009), and to the Mediterranean region (Lelieveld et al., 2002; Scheeren et al., 2003). Not only does the South Asian summer monsoon influence trace gas and aerosol particle loadings in the upper troposphere, it also affects cross-tropopause transport into the lowermost stratosphere (Traub and Lelieveld, 2003; Lelieveld et al., 2007; Randel et al., 2010; Chen et al., 2012). An extensive review on southern Asian pollution outflow in all seasons is given by Lawrence and Lelieveld (2010).

While most observations in the South Asian summer monsoon UTAC are from satellites, CARIBIC (Civil Aircraft for the Regular Investigation of the Atmosphere Based on an Instrument Container, http://www.caribic-atmospheric.com/; Brenninkmeijer et al., 2007) phase 2 provides first in situ observations over the Indian subcontinent, performed during the 2008 monsoon season. During the summer monsoon period from June through September, 14 flights between Frankfurt, Germany, and Chennai, India, were conducted, crossing the western part of the UTAC at altitudes between 10 and 12 km. The CARIBIC observatory thus contributes to the measurements within the UTAC called for by experts on atmospheric chemistry and the Asian monsoon (Crawford and Pan, 2013; Pan et al., 2014). The CARIBIC in situ observations in the upper troposphere aim to contribute to the understanding of the monsoon and its impacts on atmospheric composition through this work and previous studies which dealt with the elevated mixing ratios of a range of trace gases that were measured by CARIBIC within the UTAC, for example CO, CH_4, nitrous oxide (N_2O), sulfur hexafluoride (SF_6) (Schuck et al., 2010), several nonmethane hydrocarbons (NMHCs; Baker et al., 2011), and methyl chloride (CH_3Cl; Umezawa et al., 2014, 2015). Furthermore, as earlier measurements from CARIBIC phase 1 have shown, aerosol particle number concentrations are enhanced in the UTAC (Hermann et al., 2003). Trajectory calculations indicated that the air masses originated mainly from South Asia and mainland Southeast Asia and had been transported up to cruise altitude by deep convection associated with the summer monsoon. High mixing ratios of water vapour at southern latitudes confirmed that recent convection had occurred. An analysis of tracer correlations, namely CO, CH_4, and ethane (C_2H_6), revealed that, in addition to enhanced vertical transport of polluted boundary layer air, emissions of methane from biogenic sources, such as wetlands, open landfills, and rice paddies, increase during the summer months (Baker et al., 2012), resulting in disproportionately high mixing ratios. Carbon dioxide (CO_2) mixing ratios were found to be lower inside the UTAC. A model study using CARIBIC data found that, at least in 2008, the region was a net sink of CO_2 because of strong uptake by the terrestrial biosphere (Patra et al., 2011). Independently, observed low CO_2 mixing ratios with increased $\delta^{13}C(CO_2)$ values combined with low $\delta^{18}O(CO_2)$ values indicate photosynthetic uptake of CO_2 and oxygen atom exchange with soil and leaf water (Assonov et al., 2010).

Interestingly, the CARIBIC observatory also encountered air masses with the typical monsoon signature of elevated mixing ratios of CH_4, N_2O, SF_6, and some NMHCs, accompanied by relatively low CO_2 mixing ratios far away from the South Asian monsoon region, namely over eastern Canada in the vicinity of Toronto in September 2007. This raises the question about the whereabouts of air masses that are exported from the UTAC. Air mass trajectories pointed to export from the monsoon region (see Sect. S1 for details), although transport of Asian pollution over the Pacific towards North America occurs predominantly in the northern hemispheric winter and spring (Liu et al., 2003), whereas in summer westward outflow is prevalent. While no comparable case was observed during CARIBIC flights to North America in subsequent years, plumes of photochemically processed air originating from Asia have been probed over different parts of North America during INTEX-NA (the Intercontinental Chemical Transport Experiment – North America) flights in July and August 2004 (Liang et al., 2007).

CARIBIC measurements yield a fairly detailed description of the chemical composition of air in different parts of the UTAC, including mixing ratios of ozone precursors like the sum of reactive nitrogen oxides (NO_y), CO, and NMHCs. Using this information and the Lagrangian particle dispersion model FLEXPART (Stohl et al., 2005) we investigate the characteristics of the trapping of pollution, its distribution and the evolution of chemical composition in the UTAC. Furthermore, based on analyses of air mass forward trajectories several receptor regions are identified and their relative role for monsoon pollution export is tentatively quantified. Additional material is presented in the Supplement.

2 Methods

The CARIBIC observatory phase 2 started its routine operation in 2005 using a Lufthansa Airbus A340-600 to make measurements during sequences of typically four

Table 1. CARIBIC2 flights to Chennai, India, in 2008. Listed are the flight number, date of departure and flight direction. Column 4 gives the northern cut-off for the trajectory analysis which was selected for each month to exclude trajectories belonging to the eastward jet stream. Column 5 lists the latitude of the wind reversal along each flight track which is used as an indicator of centre latitude of the monsoon UTAC at flight altitude (see Fig. 4). The last column indicates whether air samples have been collected or not.

Flight no.	Direction	Date of departure	Northern cut-off	Monsoon centre latitude	Air samples?
236	southward	18 June 2008	36.5° N	27.9° N	yes
237	northward	18 June 2008	36.5° N	25.5° N	yes
238	southward	19 June 2008	36.5° N	25.8° N	no
239	northward	19 June 2008	36.5° N	24.4° N	no
240	southward	15 July 2008	40.0° N	26.7° N	yes
241	northward	15 July 2008	40.0° N	26.1° N	yes
244	southward	13 August 2008	40.0° N	26.6° N	yes
245	northward	13 August 2008	40.0° N	24.6° N	yes
246	southward	14 August 2008	40.0° N	25.8° N	no
247	northward	14 August 2008	40.0° N	25.3° N	no
248	southward	10 September 2008	35.5° N	23.5° N	yes
249	northward	10 September 2008	35.5° N	22.7° N	yes
250	southward	11 September 2008	35.5° N	24.9° N	no
251	northward	11 September 2008	35.5° N	24.0° N	no

long-distance flights per month. This specific aircraft was retrofitted in 2004 with a permanently mounted air and aerosol particle inlet system which is connected via (partially heated) stainless steel tubing (some of which lined with perfluoroalkoxy alkane (PFA) to reduce wall effects) to the CARIBIC container when installed (Brenninkmeijer et al., 2007). The 1.6 t container houses instruments for in situ measurements and remote sensing as well as systems for air and aerosol particle collection. In this study, results from both the in situ measurements providing a high data density along the flight track and from the air sampling equipment are used. The latter gives a low data density (28 samples per monthly flight sequence) but with more detail because many more trace gases are analysed retrospectively in the collected air samples. Flights start in Frankfurt (since August 2014 from Munich), Germany, to various destinations around the globe. After the final return flight, the container is unloaded, the measurement data are retrieved and the air samples are analysed for a suite of different trace gases in several laboratories (Brenninkmeijer et al., 2007; Schuck et al., 2009; Baker et al., 2010; O'Sullivan, 2007).

From April to December 2008, the CARIBIC container took measurements during 32 flights between Frankfurt, Germany, and Chennai, India (see list on http://www.caribic-atmospheric.com). For this study, we consider the 14 "monsoon" flights conducted between June and September 2008 (see list of flights in Table 1). These months represent the core of the monsoon period over India as previously discussed by Schuck et al. (2010) and Baker et al. (2011). More information about the non-monsoon months can be found in these two previous studies and will not be discussed here. All 14 flights crossed the western part of the monsoon UTAC between the western coast of India and Chennai at the southeast coast. The UTAC was probed at altitudes between 10.3 and 11.9 km (see Fig. S4 in the Supplement). Wind fields obtained from the European Centre for Medium-Range Weather Forecasts (ECMWF) at the 250 hPa model level, which corresponds approximately to the flight altitude, are shown as 10-day means in Fig. 1. In the north, the meandering subtropical jet is shifted northwards and slows down as the monsoon progresses northwards from June to August, while it regains strength and moves south in September as the monsoon retreats. In June, the wind arrows show the UTAC centred over northern India and Pakistan. July shows an expansion of the UTAC towards eastern China and a split of the UTAC with a second "eye" over northern Africa. In August, the centre of the UTAC is spread out over northern India, Pakistan, and the Arabian Peninsula, and with the retreat of the monsoon in September, the UTAC slowly fades and is less clearly visible in the wind field.

In addition to a suitable wind field structure provided by the monsoon UTAC, trapping pollutants also requires sources for these which are typically located at the ground (e.g. Vogel et al., 2015). Figure 2 shows emission data for CO and the sum of all non-methane volatile organic compounds (NMVOCs) from all sources listed in the Regional Emission inventory in ASia (REAS) version 2.1 (Kurokawa et al., 2013, including the November 2013 update) for August 2008 in India and the surrounding region below the UTAC and in its source region. The geographical distributions for CO (left panel) and NMVOCs (right panel) are similar in the region. The Indo-Gangetic plain in northern India and southern central China show high CO emissions together with parts of Thailand and Vietnam. NMVOC emissions are some-

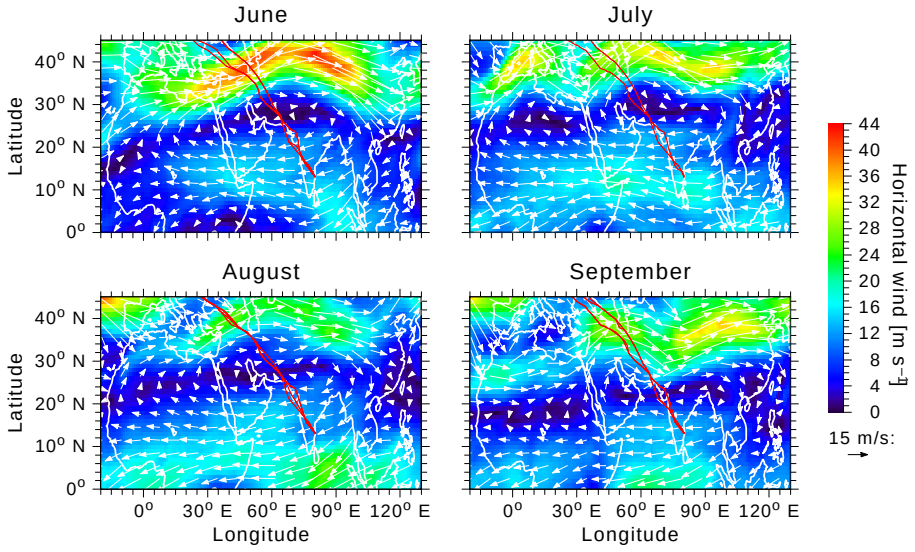

Figure 1. CARIBIC flight tracks across the South Asian monsoon region in June–September 2008. The panels show the flight tracks for each month and 10-day mean ECMWF horizontal wind fields at 250 hPa ending at the day of the last flight in each month. The colour code shows the wind speed, while the white arrows indicate the wind direction. Note the anticyclonic monsoon circulation centred over the Indian subcontinent.

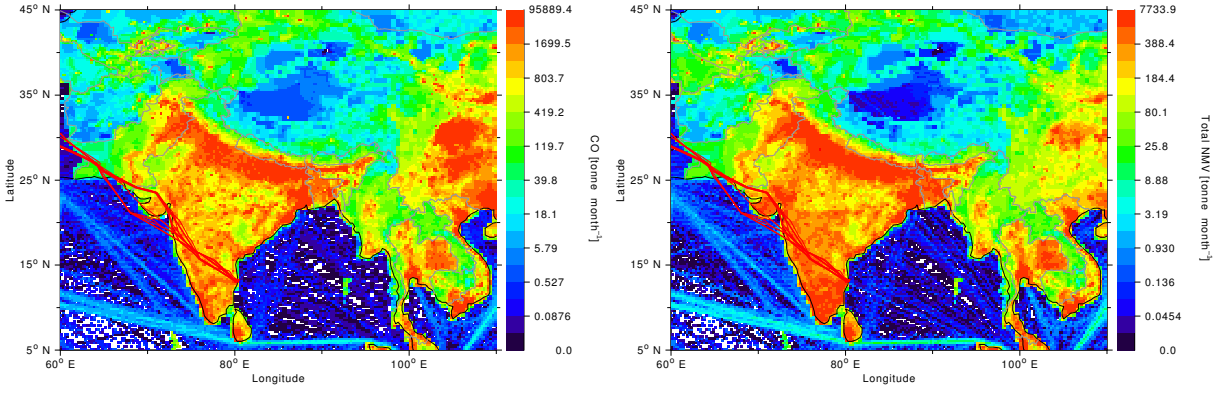

Figure 2. Emissions of CO (left panel) and non-methane volatile organic compounds (right panel) for August 2008 from the Regional Emission inventory in ASia (REAS) v2.1 (Kurokawa et al., 2013) including the update from 14 November 2013. The red lines mark the CARIBIC flight tracks for June to September 2008.

what higher in southern India and lower in southern central China compared to CO emissions. Detailed modelling studies with the Weather Research and Forecasting with Chemistry (WRF-Chem) online regional chemistry transport model to link emissions and transport have been published separately (Ojha et al., 2016).

2.1 CARIBIC trace gas and aerosol measurements

The CARIBIC container houses a number of different instruments for measuring a spectrum of trace gases and also aerosol particles (Brenninkmeijer et al., 2007). Discussed extensively in this work are CO, O_3, NO_y, and aerosol particles (N_{4-12} and N_{12}). Brief descriptions of these measurements are presented next.

Carbon monoxide is measured with an AeroLaser AL 5002 resonance fluorescence UV instrument modified for use onboard the CARIBIC passenger aircraft. The instrument has a precision of 1–2 ppbv at an integration time of 1 s and performs an in-flight calibration every 25 min. A technical description of the CO instrument can be found in Scharffe et al. (2012).

Ozone measurements are based on a fast, commercially available dry chemiluminescence (CL) instrument, which has a precision of 0.3–1.0 % at typical ozone mixing ratios between 10 and 100 ppbv and a measurement frequency of 10 Hz . The performance of this instrument has been char-

acterised in detail by Zahn et al. (2012). The absolute ozone concentration is inferred from a UV photometer designed in-house which operates at 0.25 Hz and reaches an accuracy of 0.5 ppbv.

The sum of reactive nitrogen oxides (NO_y) is determined using an NO chemiluminescence detector (Eco Physics AG) after conversion of NO_y to NO (Ziereis et al., 2000). The time resolution is 1 s. The overall uncertainty for the NO_y measurement at 10 s time resolution is about 7 % at 450 pptv NO_y (Brough et al., 2003).

The total water mixing ratio (gaseous, liquid, and ice phase) is measured by means of a chilled-mirror frost-point hygrometer (CR-2, Buck Research Instruments L.L.C.) with a time resolution of 5 (high humidity) to 300 s in the dry lowermost stratosphere with an uncertainty of around 0.3 ppmv at cruise altitude. A modified two-channel photoacoustic diode-laser spectrometer (Hilase, Hungary) measures both gaseous (H_2O_{gas}) and total water mixing ratios with a time resolution of 3 s and a precision of 1 ppmv. These measurements are calibrated to the absolute water mixing ratios determined with the frost-point hygrometer. A detailed description of the CARIBIC humidity measurements is available in Dyroff et al. (2015). An overview of the H_2O data can be found in Zahn et al. (2014).

Integral aerosol particle number concentrations are measured with three condensation particle counters (CPC, modified TSI model 7610) with lower threshold diameters (50 % counting efficiency) of 4, 12, and 18 nm, respectively, and an upper detection limit of around 2 µm at 200 hPa operating pressure (Hermann and Wiedensohler, 2001). The difference in counts between the 4 and 12 nm channels is given as N_{4-12} and corresponds to the nucleation mode. In the upper troposphere, where the CARIBIC aircraft is taking measurements, the 12nm channel (N_{12}) mainly corresponds to the Aitken mode. All aerosol particle number concentrations used in this paper are given at standard pressure and temperature (STP) of 273.15 K and 1013.25 hPa.

Whole air samples are collected in two units, each of which contains 14 glass sampling flasks of 2.7 L volume, pressurised to $\sim$ 4.5 bar during collection. Samples were collected at pre-determined, evenly spaced intervals of roughly 35 min ($\sim$ 480 km) with filling times between 0.5 and 1.5 min ($\sim$7–22 km). In months with four flights between Frankfurt and Chennai, i.e. June, August, and September 2008, sample collection only took place during the first two flights in order to achieve higher spatial and temporal resolution (see last column in Table 1). Greenhouse gases (GHGs) and NMHCs were measured post-flight in the laboratory at the Max Planck Institute for Chemistry in Mainz, Germany. GHGs are separated with a gas chromatography (GC) system and then measured by flame ionisation detection (CO_2 and CH_4) and electron capture detection (ECD, N_2O and SF_6; Schuck et al., 2009), while the NMHCs are separated on a second GC system and then measured by ECD (Baker et al., 2010).

2.2 FLEXPART trajectory calculations

FLEXPART is a widely used Lagrangian particle dispersion model in ongoing development at the Norwegian Institute for Air Research (NILU). It simulates long-range and mesoscale transport, diffusion, dry and wet deposition, and radioactive decay of various tracers (see detailed description in Stohl et al., 2005). An updated description of the FLEXPART model is available from Stohl et al. (2010). In the current study, FLEXPART version 9.02 was used together with ECMWF meteorological input data with a temporal resolution of 3 h and a spatial resolution of $1.0° \times 1.0°$ and 91 model levels.

We started trajectories every 3 min along the flight tracks and calculated them 14 days forward and backward in the single-trajectory mode of FLEXPART with enabled parameterisations for the sub-grid terrain effect and sub-grid convection. The trajectory positions were recorded every 30 min. The southernmost point of our flight track is Chennai (12.99° N, 80.18° E). The northern cut-offs for the trajectory analysis are 36.5° N in June, 40.0° N in July and August, and 35.5° N in September (see Table 1) and were chosen to exclude the subtropical jet stream and thus concentrate the analysis on the monsoon region. The continuous trace gas measurements were averaged over 60 s centred around the start points of the trajectories along the flight track to obtain representative trace gas concentrations for the air characterised by the trajectories.

3 Results and discussion

We will first present the CARIBIC observations of trace gases and aerosol particles (Sect. 3.1.1) with their latitudinal and photochemical distributions and characteristics (Sect. 3.1.2). The vertical profiles measured by CARIBIC over Chennai are presented next (Sect. 3.1.3). Then we show the origins of these air masses (Sect. 3.2) and continue with a description of where the air is transported to after it has spent time in the monsoon UTAC and how long it remains trapped inside it (Sect. 3.3).

3.1 CARIBIC observations

The following sections discuss the CARIBIC observations and how the latitudinal and vertical variations in the trace gas mixing ratios can be used to infer information about the chemical properties of the observed air masses and their origin.

3.1.1 Measurement position in the upper troposphere anticyclone (UTAC)

Along routes between Chennai and Frankfurt during the monsoon season (June–September 2008), the aircraft passed from the southern section of the UTAC, where winds are

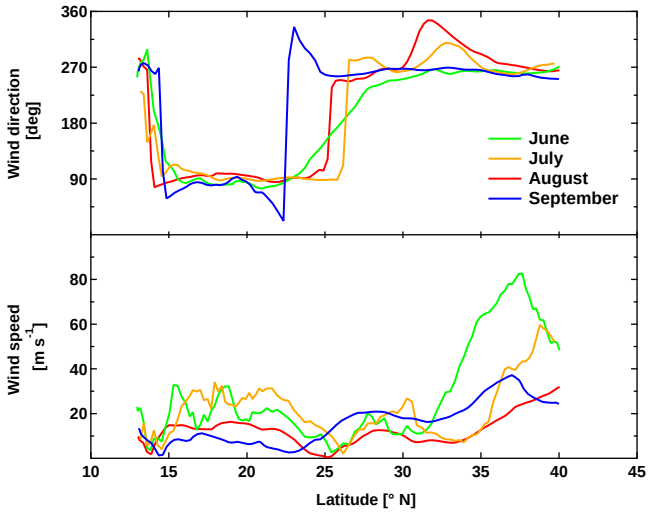

Figure 3. Latitudinal profiles of wind direction (top panel, 90° means wind from the east, 180° from the south, 270° from the west) and wind speed (bottom panel) at aircraft cruise altitude for the first flight from Frankfurt to Chennai in each of the four monsoon months.

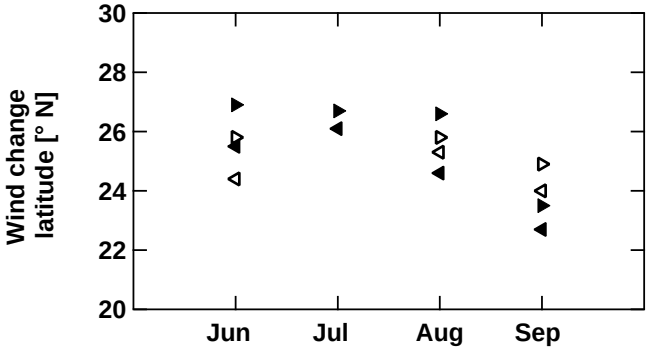

Figure 4. Latitude of the aircraft at the transition between eastward and westward flow in the UTAC for each flight during the summer monsoon 2008. Arrows pointing to the right indicate flights from Frankfurt to Chennai; arrows pointing to the left indicate return flights. Filled symbols represent the first round-trip flight series; open symbols indicate the second (when applicable). For each of the seven pairs of flights the wind change (transition point) is about 1° further north on the flight to Chennai (when the aircraft cruise altitude is 1–2 km higher) than on the return flight.

from the east, through the centre into the northern section, where winds are from the west or vice versa for flights from Frankfurt to Chennai. The transition between the two regimes is evident in the wind data recorded by the aircraft (Fig. 3), which show abrupt wind direction reversals in the vicinity of 26° N. Wind speeds are low in the centre of the UTAC (reaching near zero at the transition point) and increase strongly at the northern edge of the UTAC and upon entering the Northern Hemisphere subtropical jet stream (see also flight tracks in Fig. 1). The latitude at which the aircraft crosses between the two sections or regimes varies from month to month, with the northernmost average location in July and the southernmost in September (Figs. 3, 4, and Table 1). It is noted that there are differences observed between flights in each single month, with the point of transition on the flights to Chennai being systematically further north than on the corresponding return flights. The systematic differences in altitude expose a vertical structure in the UTAC. The cruise altitudes of the aircraft at 22–28° N for flights to Chennai are 1–2 km higher (since most aircraft fuel has already been burned) than during the return flights (when the aircrafts fuel tanks are still full shortly after take-off; see Fig. S4). However, the flight routes to and from Chennai between 22 and 30° N for each month were identical with the exception of one return flight in August (Fig. S5 in the Supplement). This implies that the differences observed between individual months (at the same altitude) document changes in the structure of the monsoon circulation (in the horizontal and/or the vertical direction). The observed northwards shift of the UTAC centre at higher altitude means that we observe an interesting northward tilt of the monsoon axis, consistent with previous work (e.g. Randel and Park, 2006, their Fig. 2). In general, the centre of the UTAC is observed to be furthest north during July (Fig. 4). This is consistent with meteorological studies of monsoon development and its northward propagation and recession (IMD, 2009).

To compensate for biases attributable to variations in flight routes and/or horizontal movements of the monsoon UTAC, and to normalise for position within the UTAC between months, we give our data an additional latitudinal coordinate. Relative latitude (Δlat) defines the location relative to the latitude at which the aircraft crosses from the northern to the southern section of the UTAC or vice versa (i.e. relative to the "centre" of the UTAC indicated by the reversal of the zonal wind). Positive Δlat describes measurements in the north, while negative Δlat describes measurements in the south, with values determined on a per flight basis.

3.1.2 Latitudinal transects

As an example for the UTAC being fully developed, Fig. 5 gives the individual trace gas, aerosol particle, and wind latitude transect profiles for the second flight from Frankfurt to Chennai in August (14 August 2008) at altitudes of 10.3 to 11.9 km between approximately 14 and 40° N. The southern section of the flight track (14–25° N) is characterised by low O_3 (Fig. 5a, average value 39 ppb for Δlat -7.5 to $-2.5°$), considering that the mean concentrations over all flights lie between 51 ± 11 (Δlat -7.5 to $-2.5°$) and 81 ± 13 ppb (for the northern part, Δlat 2.5 to 7.5°) and low NO_y (Fig. 5b, average value 0.33 ppb with corresponding mean concentrations of 0.57 ± 0.38 and 0.83 ± 25 ppb) concomitant with high CO (Fig. 5a, average value 96 ppb with corresponding mean concentrations of 101 ± 8 and 92 ± 10 ppb), high water vapour (Fig. 5b, av-

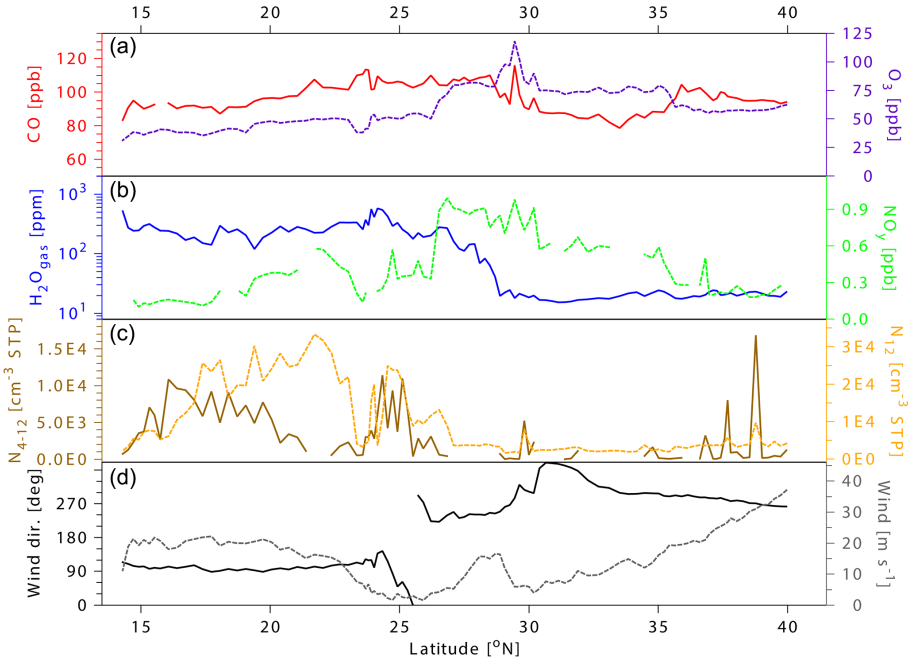

Figure 5. Latitudinal profiles of trace gases and meteorological parameters during the second flight in August from Frankfurt to Chennai on 14 August 2008. In addition to colour coding of axes, scales for parameters represented by solid lines are on the left and scales for parameters represented by dashed lines are on the right. Aerosol particle number concentrations are given at STP (273.15 K, 1013.25 hPa). Note that all data are shown versus geographical latitude and that the water vapour shown in blue in **(b)** is on a logarithmic scale (see also Figs. S9–S21 in the Supplement).

erage value 299 ppm with corresponding mean concentrations of 409 ± 219 and 35 ± 41 ppm) and high aerosol particle number concentrations (Fig. 5c). In the northern section (27–40° N), the opposite is observed; mixing ratios of O_3 (average value 86 ppb for Δlat 2.5 to 7.5°) and NO_y (average value 0.81 ppb) are elevated, while levels of CO are a little higher for this flight (average value 102 ppb). Here especially the levels of water vapour and aerosol particle number concentrations are much lower, with the exception of some brief instances of elevated nucleation-mode (N_{4-12}) particle number concentrations. These distinct and clear patterns are observed for all flights under investigation in all months and are attributable to the influence of different air mass source regions, different chemical regimes, and varying transport times within the different regions of the UTAC (see also Fig. 6 below and Figs. S9–S21 in the Supplement).

An important feature of the monsoon is persistent deep convection over South Asia, which is strongest over the Bay of Bengal and the Indian subcontinent (Devasthale and Fueglistaler, 2010). South of $\sim 26°$ N (Δlat < 0) the aircraft encountered air that had passed over these highly active convective regions and had become burdened with emissions from South Asia. This accounts for enhancements in the primary pollutant CO and relatively low levels of the secondary pollutant O_3, as well as the enhancements in water vapour. Likewise, high levels of nucleation-mode aerosol particles (i.e. freshly formed particles, N_{4-12}) persisted. These aerosol particles are very short-lived relative to the other species (hours to a few days) and can be regarded as indicators of convection (Weigelt et al., 2009). Interestingly, mixing ratios of NO_y are lower in the south than in the north (0.37 vs. 0.72 ppb), possibly as a result of lower NO_x emissions in the south combined with the conversion to water-soluble components of NO_y in the highly reactive polluted air masses followed by enhanced removal under the high-temperature, high-humidity conditions of the monsoon. In the north, the air parcels encountered by CARIBIC have been transported for several days within the UTAC and show signs of chemical processing and aging. Water vapour and nucleation-mode particles have been depleted by experiencing low temperatures during transport and washout, respectively. CO levels are reduced and O_3, given more time to form photochemically, is elevated. Similar changes in composition could have been caused by in-mixing of stratospheric air. However, care has been taken to identify and remove all data points that have stratospheric influence based on the measured ozone concentrations and the potential vorticity (PV) values from the ECMWF model using thresholds of 150 ppb and 1.3 PVU for ozone and PV, respectively. The distinction between freshly polluted air in the southern section and more processed, aged air in the northern section is also supported by a previous study of CARIBIC NMHC data (Baker et al., 2011).

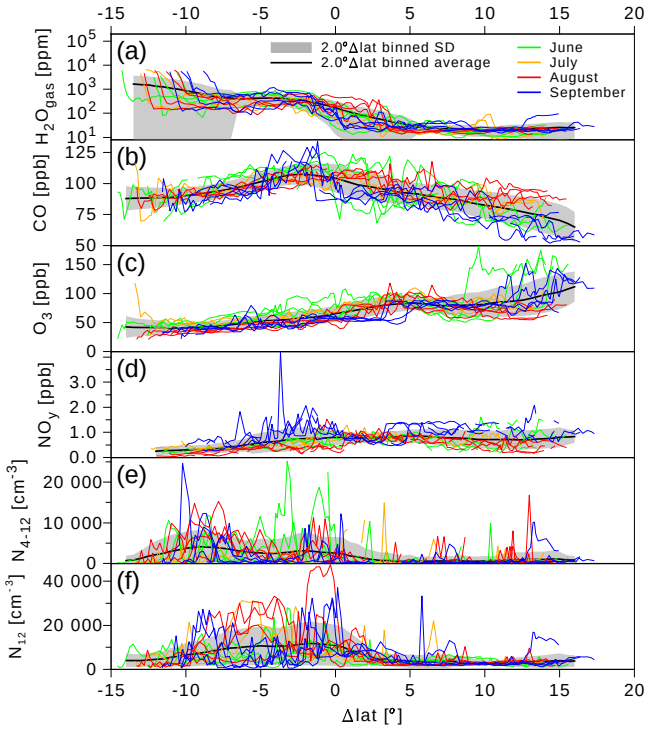

Figure 6. Profiles of trace gases **(a–d)** and aerosol particle number concentrations (**e** and **f**, at STP 273.15 K, 1013.25 hPa) vs. relative latitude (Δlat) coordinates for all flights. The colours indicate the flight month, the black line is the mean over all flights, and the grey shading indicates the 1σ standard deviation around the mean (both calculated over moving 2° Δlat bins). Note the logarithmic scale in the water vapour plot in **(a)**.

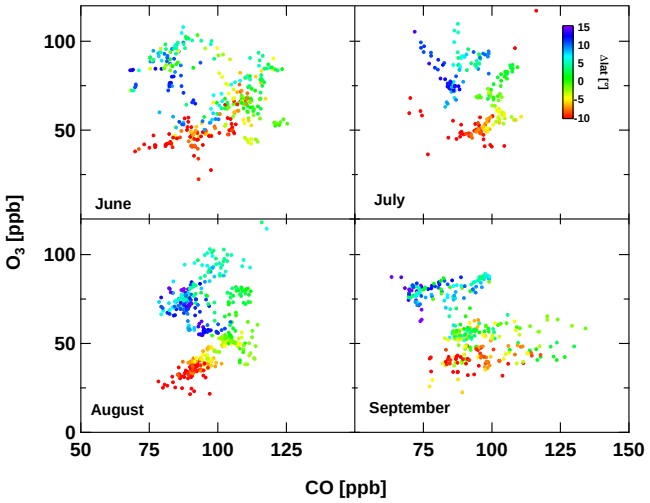

Figure 7. Monthly distributions of O_3 vs. CO during the summer monsoon season 2008. Points are colour-coded by relative position within the UTAC, as determined by Δlat (see also Sect. S6 in the Supplement).

Results for all individual flights are plotted against relative latitude in Fig. 6. The standard deviation calculated over moving 2° relative latitude bins is shown as grey shading. Water vapour in Fig. 6a is shown on a logarithmic scale. The differences of the means for the southern and northern section of the flights are larger than the 1σ standard deviation (see numbers given above) for all trace gases except for CO, which shows a maximum slightly south of the wind reversal (Δlat ∼3°) decreasing southwards and northwards. In general, trace gas (Fig. 6a–d) and aerosol particle concentration (Fig. 6e and f) profiles in June, July, August, and September are similar, although the overall patterns are interrupted by certain events. Notable features are the much higher NO_y (Fig. 6d) and lower CO (Fig. 6b) in the north during September (with no notable difference for O_3), and the abrupt gradient in CO concentrations between north and south during June. The large variability in aerosol particles compared to the trace gases is caused by the strong dependency of the particle number concentration on clouds whose position relative to the CARIBIC flight tracks was different during each flight. Monthly mean aerosol particle distributions by latitude are shown in Sect. S5 in the Supplement. A detailed investigation of clouds and particle number densities is beyond the scope of this work and the interested reader is referred to the CARIBIC-based work by Weigelt et al. (2009).

As our analysis focuses on the monsoon as a transport mechanism for polluted air masses from South Asia and mainland Southeast Asia and the influence on other regions, understanding the composition and chemistry of air parcels as they move through the UTAC is critical for evaluating the potential impact on downwind regions. This includes understanding not only of primary pollutants in transported air masses but also of the tendency to form secondary pollutants, particularly ozone. A previous CARIBIC data-based study of the relationship between ozone and NMHCs, which are indicators of pollution and act to some degree as ozone precursors, showed that air masses in the south have a greater ozone formation potential than in the north, where air masses have diminished formation potential or show the beginnings of ozone destruction (Baker et al., 2011). Ozone formation potentials in the troposphere can also be qualitatively understood through the relationship between ozone and carbon monoxide using the enhancement ratio $\Delta O_3/\Delta CO$ (Fishman and Crutzen, 1978; Parrish et al., 1998; Zahn et al., 2002), as determined from correlation plots, in addition to the information provided by the coarser resolution NMHC data. Positive correlations, i.e. $\Delta O_3/\Delta CO > 0$, indicate the formation of ozone. Negative correlations can (outside of stratospheric influence) indicate destruction of ozone or in-mixing of different air masses, which may also apply when a lack of correlation is observed (Parrish et al., 1993; Trainer et al., 2000; Voulgarakis et al., 2011, and references therein).

Figure 7 shows scatter plots of O_3 vs. CO during each of the four monsoon months with colour coding indicating

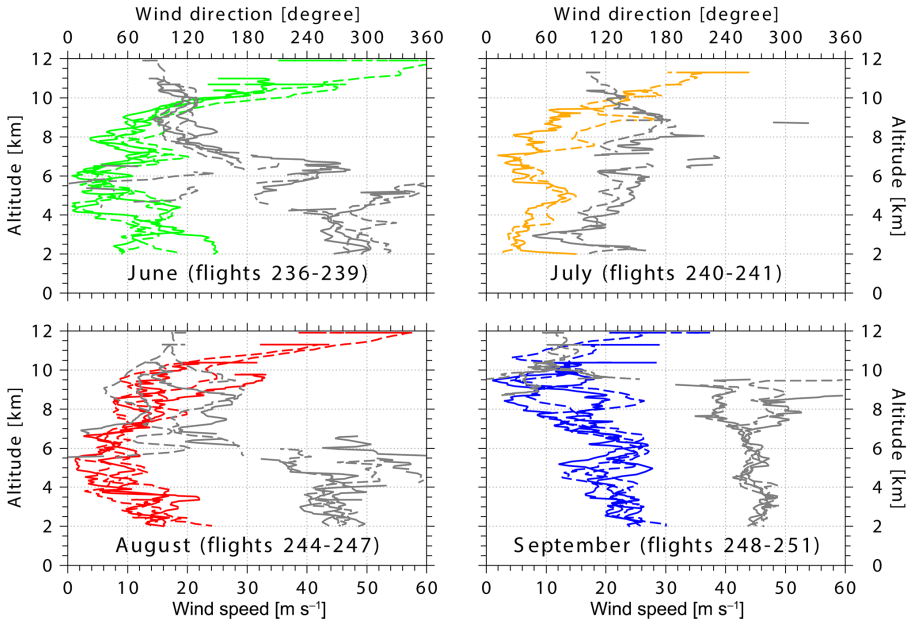

Figure 8. Wind speed (coloured lines, lower x axis) and wind direction (grey lines, upper x axis, 90° means wind from the east, 180° from the south, 270° from the west) as recorded by the CARIBIC aircraft for the descent into (solid lines) and ascent from (dashed lines) Chennai. Only data south of 16° N and above 2 km altitude are plotted. Chennai is at 12.99° N, 80.18° E.

relative latitude. First of all, the low-latitude data ($-10° < \Delta\text{lat} < -5°$) combine low O_3 values (< 50 ppb) with about 75–100 ppb CO. With the exception of September (which has few statistically significant slopes at all in the low-latitude band) the $\Delta O_3/\Delta CO$ slopes are significant and positive. At the northern edge of the UTAC ($\Delta\text{lat} \sim 15°$), again with the exception of September, slopes are negative, whereas August has positive values throughout except for $\Delta\text{lat} < 15°$. The correlation slopes north of $-5°$ vary considerably. Here O_3 values are definitely higher; they are, however, not well correlated with the generally similar CO values between 75 and about 110 ppb. These relationships for the monsoon months indicate that ozone-forming regimes dominate in the south, while in the northern part of the UTAC there is no clear potential for ozone formation (see also Sect. S6 and Fig. S25 in the Supplement, which shows the values of the slope as a function of relative latitude). All these tendencies are determined from the slope of $\Delta O_3 / \Delta CO$ over a few degrees latitude, which agrees with the range of 200–500 km used in an earlier study by Zahn et al. (2002, their Fig. 10). As expected, correlations for the individual flights (not shown) yield similar qualitative results since the time between the individual flights through the monsoon in one month is short (12–36 h) compared to the transport time of the air inside the UTAC (many days).

3.1.3 Vertical profiles over Chennai

The majority of flight time through the UTAC was spent at cruise altitude in a narrow altitude range between 10.3 and 11.9 km (see Fig. S4 in the Supplement), providing limited insight into the vertical distribution of trace species in the UTAC. However, the descent into and ascent from Chennai airport provide us with some information in the vertical in the southern part of the UTAC, as the aircraft passes between $\sim$ 11 km and ground level over a relatively short distance ($\sim$ 200–250 km) in approximately 30 min (Fig. S4 in the Supplement). During this time the aircraft moves from being within the UTAC into the free troposphere below and eventually into the boundary layer and vice versa. In situ data are available for most species down to $\sim$ 2 km, with the exception of water vapour, which is available down to $\sim$ 5 km only, and NO_y, which is not available below $\sim$ 10 km. Aerosol particle number concentrations during ascent are only available above 6 km. No whole air samples were collected on ascent and descent. Both ascent and descent took place during night, with landing times around 23:30 LT (local time) and take-off between 02:00 and 03:40 LT the following morning (Fig. S4 in the Supplement). Descents into the airport were from a west–north-west direction towards the Bay of Bengal and final approaches from the east while the ascents were over land west of Chennai (except for the September flights, which took off to the east). Similar flight times and patterns were followed for all flights except for July, when the approach into Chennai followed a route further north of Chennai before the final approach to the airport from the east (see Fig. S6 in the Supplement).

While descending from cruise altitude, the aircraft moved from the westward flow of the UTAC into the eastward flow of the low-level Somali Jet with its wind speed maximum

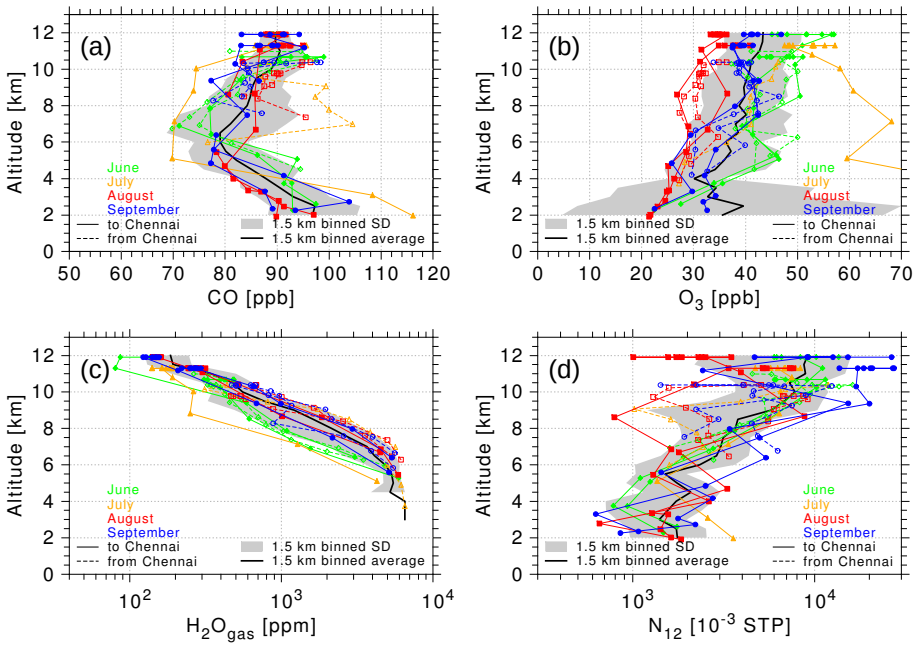

Figure 9. Vertical profiles of CO **(a)**, O_3 **(b)**, water vapour **(c)**, and number concentration of Aitken-mode aerosol particles N_{12} at STP (273.15 K, 1013.25 hPa) (**d**) between 2 km and 12 km during descent into (solid lines and filled symbols) and ascent from (dashed lines and open symbols) Chennai. The colours indicate the flight month, the black line is the mean over all flights, and the grey shading indicates the 1σ standard deviation around the mean (both calculated over moving 1.5 km altitude bins). Note the logarithmic x axis for water vapour **(c)** and aerosol particles **(d)**.

around 850 hPa (Chakraborty et al., 2009). This is clearly visible in the wind direction recorded by the CARIBIC aircraft shown in Fig. 8. In June and August this transition occurred between 6 and 7 km, while in September it was around 9 km altitude. In July, tropospheric wind speeds were much lower than in the other months and there was no wind reversal evident from the measurements. This was a general feature of the meteorology on 15 and 16 July when the flights took place. Over a large region in southeastern India and out over the adjacent Bay of Bengal, wind speeds were very low from the surface up to 500 hPa ($\sim$ 5 km), which is about the height of the wind reversal seen in Fig. 8 in June and August. The corresponding ECMWF wind fields during the days of the flights are shown in Fig. S7 (745 hPa winds) and Fig. S8 (510 hPa winds) in the Supplement. Over central India and the Indian Ocean south of India there were eastward winds in the lower troposphere extending the Somali Jet over the Indian subcontinent and into the Bay of Bengal. But just around Chennai, winds were very calm. This has probably led to a trapping of the local pollution from the city of Chennai during these days in July 2008, whereas higher wind speeds in the lower troposphere were encountered in the other months.

Vertical trace gas and aerosol particle profiles during descent and ascent show a fairly consistent picture, although trace gas data for the two July flights (see orange lines in Fig. 9) reflect the unique meteorological situation described above, particularly during the descent into Chennai. Very dry conditions (Fig. 9c) were measured while O_3 was strongly enhanced (Fig. 9b) and further increased with decreasing altitude, reaching 116 ppb at the lowermost point (not shown). These profiles were also characterised by high CO (Fig. 9a) between 6 and 9 km, which is above the level of wind direction change. There was no recognisable change in the number concentration of Aitken-mode aerosol particles (Fig. 9d). In the free troposphere there was a weak north-westward flow (see Fig. 8) which would transport the pollution of Chennai and its industries right to the region where the July flight descended into Chennai airport (see Fig. S6 in the Supplement), while the other flights descended from the west–north-west, i.e. mostly upstream of the pollution sources in Chennai.

In the other months, vertical "C-shaped" profiles of CO (see Fig. 9a) reflect the position change outside and inside of the UTAC as the aircraft ascends into the upper troposphere. Moving upward from 2 km, mixing ratios of CO decrease until reaching the point where the wind direction changes, marking entry into the lower levels of the UTAC. Here, CO begins to increase, often reaching, and even exceeding, maxima observed at lower altitudes. The difference between maximum and minimum is most pronounced in June, with mixing ratios in the middle troposphere being higher than in the other months, when mixing ratios are fairly similar. No significant differences between ascents and descents are observed. The standard deviation calculated over

moving 1.5 km altitude bins is shown as grey shading and supports the "C-shaped" profile.

Profiles of O_3 (Fig. 9b) show increasing mixing ratios with altitude, with no clear transition between free troposphere and UTAC and no significant differences between ascent and descent. A monthly trend is present, with the lowest values in August and the highest values in June, when the vertical gradient was also steepest. Monthly differences are most pronounced above 6 km. Conversely, water vapour (Fig. 9c) decreased with altitude, with a similar vertical gradient during each month. June profiles were the driest, with the exception of the second flight into Chennai in September and the flight into Chennai in July (see above). June is at the beginning of the monsoon season in India, when precipitation is not yet as strong as during the subsequent months.

Concentrations of the Aitken-mode aerosol particles (N_{12}, Fig. 9d) show a positive vertical gradient, except for one descent in August, which is variable with altitude but shows no consistent trend. There are no significant monthly differences in concentration or gradient. Also, N_{12} particle number concentrations during ascent and descent are more or less equal considering their general variability with altitude. This is expected since both descent and ascent occur well after nightfall, when all direct influence from the daytime convective activity has ceased. Part of the variability of the vertical N_{12} profiles is due to crossing of contrails of other aircraft with locally very high aerosol particle number concentrations.

Measurements of O_3 profiles with MOZAIC (Measurement of OZone by Airbus In-service airCraft) aircraft over Chennai in 1996 and 1997 (Sahu et al., 2011) and Hyderabad in central India in 2006–2008 (Sahu et al., 2014) showed similar concentrations and a similar positive gradient with altitude. However, none of these observations documented a large increase towards the surface in the monsoon months as observed by CARIBIC in July 2008. MOZAIC CO profiles measured over Hyderabad in 2006–2008 (Sheel et al., 2014) were more or less constant at $\sim$ 100 ppb throughout the free and upper troposphere and only showed an increase towards the surface below $\sim$ 4 km. A pronounced increase in CO in the free troposphere as measured by CARIBIC in July 2008 was not observed over Hyderabad in the summer months of these years. This corroborates that 15/16 July 2008 was an exceptional case with respect to the CO and O_3 profiles over Chennai.

3.2 Source regions of monsoon air

Before dealing with the fate of the air masses probed by CARIBIC (Sect. 3.3) we investigate the origin and subsequent processing of pollution during the trapping in the UTAC at low temperatures, pressures, and water vapour under high insolation. In previous CARIBIC papers we have discussed the issue of the origin of certain pollutants (Schuck et al., 2010; Baker et al., 2011, 2012). Figure 10 shows trajectories calculated with the FLEXPART model for a representative case to identify the origin of the air that was sampled by the CARIBIC aircraft when flying through the UTAC. The backward trajectories for the flight to Chennai on 13 August 2008 are colour-coded with trajectory altitude above sea level. As the trajectory reliability decreases with time into the past (and future), we use only the first 10 days for the source and receptor region analysis and in all subsequent plots.

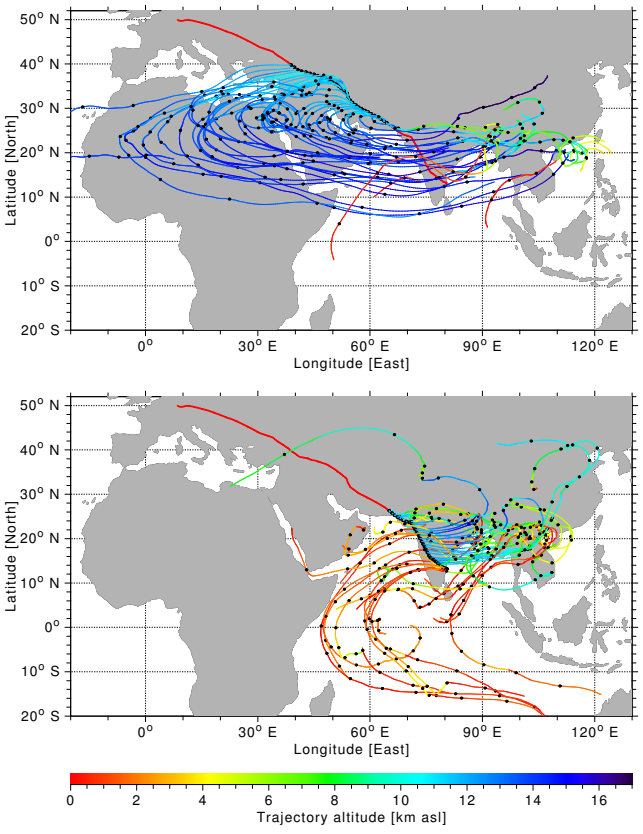

Figure 10. Ten-day backward trajectories for CARIBIC flight 244 to Chennai on 13 August 2008. Upper panel: trajectories north of the wind reversal at 26.6° N. Lower panel: trajectories south of the wind reversal. Every second trajectory is plotted for clarity. The colour indicates the trajectory altitude (in km above sea level) and the black dots mark 24 h time steps along the trajectories. The CARIBIC flight track is shown by the thick red line.

For the northern section of the flight track most of the observed air masses, approaching from the west, have resided for 4 days or longer inside the UTAC at altitudes (indicated by the trajectory colour in Fig. 10) at or above the CARIBIC flight altitude. For the southern section, the air masses reached the CARIBIC flight track from the east after having been convected over or east of the Bay of Bengal, originally having followed an eastward flow in the lower troposphere with the Somali Jet over the Arabian Sea and central and southern India. Only when approaching Chennai airport at low altitudes we observed air coming directly from the west without having passed over the Bay of Bengal.

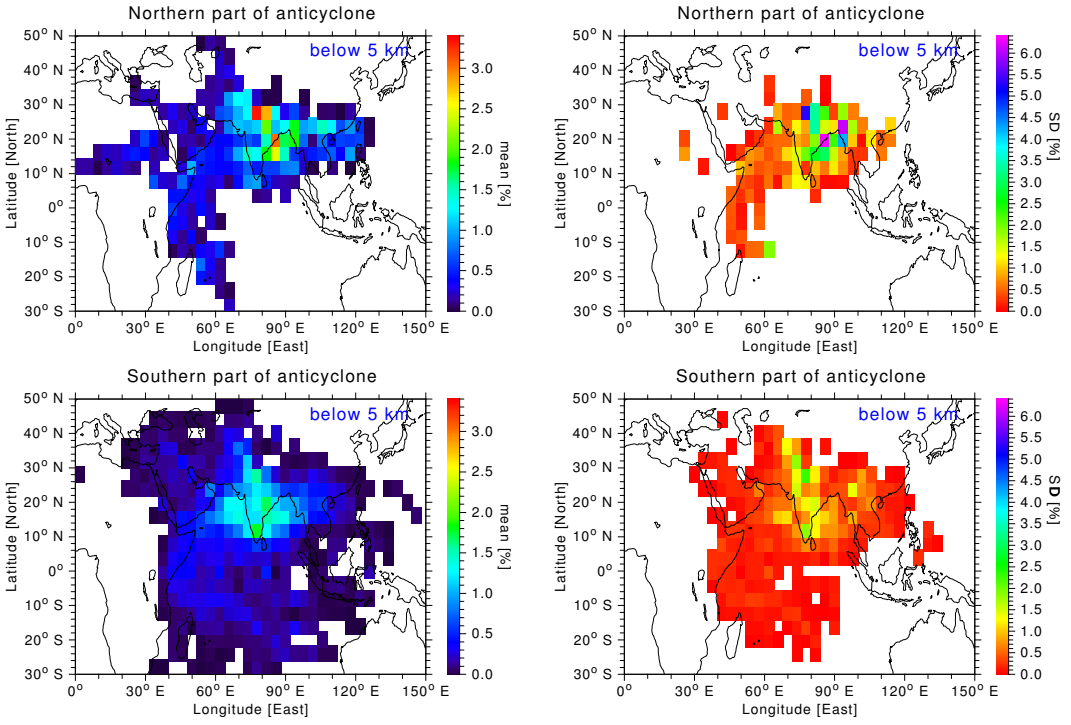

Figure 11. Distribution of source regions for all the CARIBIC flights. The colour code shows the percentage of trajectory points that were below 5 km altitude in the preceding 10 days per $4° \times 4°$ grid box. Upper left panel: source regions for trajectories starting north of the wind reversal. Lower left panel: source regions for trajectories starting south of the wind reversal. Right panels show the corresponding standard deviation of the percentages in the monsoon months June to September per grid box for all grid boxes reached by trajectories from at least 2 months (see also Figs. S26–S29).

Table 2. Receptor regions used in the analysis of the FLEXPART forward trajectories.

Name	Region
North America	30–50° N, 150–70° W
Central Pacific	10–34° N, 130° E–150° W
Central Africa	0–25° N, 10° W–35° E
Mediterranean	28–40° N, 0° E–40° W
South Asian monsoon	centre: 80° E*; radius: 38° longitude, 16° latitude
TP stratosphere	higher than thermal tropopause along trajectory
PV stratosphere	higher than dynamical tropopause (PV > 2.5 PVU) along trajectory

* Latitude of monsoon centre is flight-dependent (see second-to-last column in Table 1).

A summary of the source regions for all flights is shown in Fig. 11 by means of the geographical distribution of all points of the backward trajectories below 5 km altitude, i.e. in the lower troposphere (left panels). The right panels show the corresponding 1σ standard deviation of the percentages over the monsoon months June to September. The limit of 5 km was chosen because it is well below altitude of the wind reversal which separates the upper troposphere region with the monsoon UTAC from the lower troposphere (see also Fig. 8). Lower-altitude thresholds (down to 1 km, not shown) do not change this picture significantly. This points to rapid more or less directly vertical convection from the lower troposphere into the UTAC region. For the northern part of the UTAC (upper left panel), the air came from eastern India, the Indo-Gangetic Plain, and from the northern parts of the Bay of Bengal and mainland Southeast Asia. The air measured in the southern part of the UTAC (lower left panel) originated in central and southern India, the western part of the Bay of Bengal, and the Arabian Sea off the western coast of India. The 1σ standard deviations per grid box (right panels in Fig. 11) scale with the mean distribution – i.e. a high mean value is most often accompanied by a high standard devia-

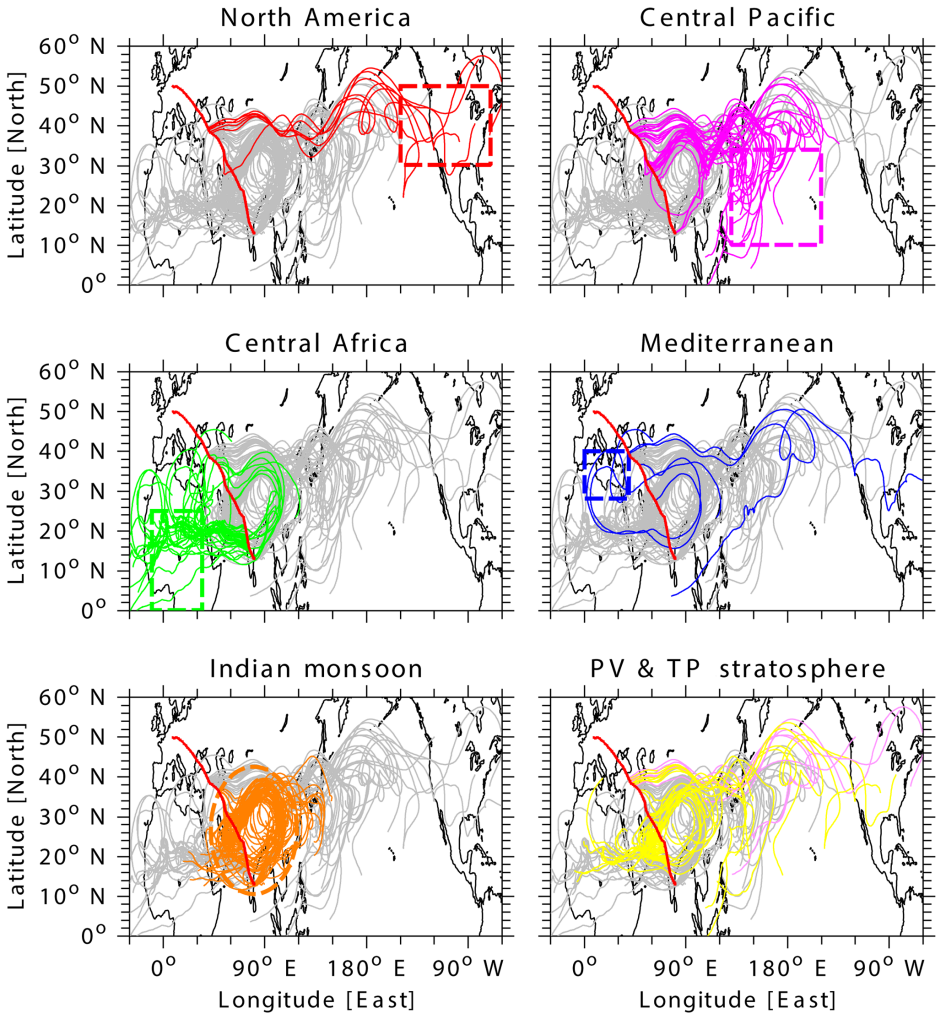

Figure 12. Receptor regions as determined for CARIBIC flight 244 to Chennai on 13 August 2008 (flight track shown with thick red solid line). The panels show all FLEXPART forward trajectories for this flight south of the northern cut-off (40° N) in grey. For each receptor region, the corresponding trajectories are shown in colour. The dashed lines indicate the boundaries of the receptor regions (boxes and ellipse). Trajectories with stratospheric parts are shown in the lower right panel in yellow for the thermal and pink for the dynamical tropopause criterion.

tion. This shows that the position of the convective events is variable – i.e. a grid box with a high percentage in one month may have a lower mean percentage in the next month when the high percentage may be found in the neighbouring grid box. While the general pattern was similar for the all flights in June–September 2008, the exact location of the convective uplift and hence the detailed pattern of the source regions varied (see Figs. S26–S29 in the Supplement).

3.3 Outflow from the UTAC

The following subsections describe the fate of the air and the contained trace species observed with CARIBIC after they have been processed in the monsoon UTAC.

3.3.1 Receptor regions of monsoon air

FLEXPART forward trajectories were used to determine to where the air masses observed by CARIBIC at cruise altitude in the South Asian monsoon UTAC were transported. We defined seven receptor regions, listed in Table 2. Over North America, central Pacific, central Africa, and the Mediterranean, we defined boxes reaching from the ground to the thermal tropopause. The trajectories are detected over these regions if they are within the defined boxes using the local thermal tropopause height output from the FLEXPART model along the trajectories. The South Asian monsoon region itself is defined as an ellipse with the centre at 80° E, while its latitude is between 22.7 and 27.9° N depending on the actual flight (see second to last column in Table 1). The

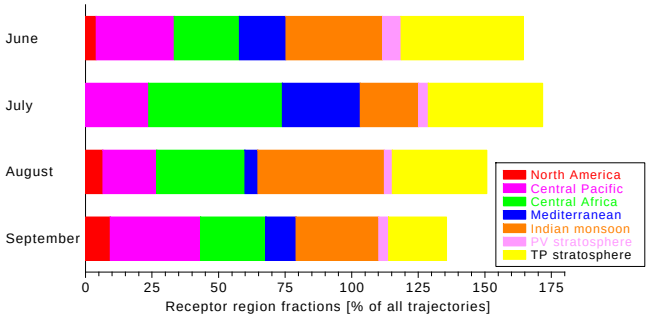

Figure 13. Receptor region fractions averaged over all CARIBIC flights to Chennai in June to September 2008. Since trajectories may reach multiple receptor regions, the totals exceed 100 %.

monsoon centre latitude is determined from the zonal (west–east) wind reversal along the flight track using the wind speed and direction recorded by the aircraft (see Sect. 3.1.1). To qualify as a monsoon trajectory, the trajectory has to stay for at least 70 % of the 10-day period within the monsoon ellipse and below the thermal tropopause. Trajectories which stayed for at least 24 h above the thermal or dynamical tropopause (PV > 2.5 PVU) were counted as TP (tropopause) or PV stratospheric trajectories, respectively. As expected, all but one of the trajectories which met the criterion for the dynamical tropopause also met the criterion for the thermal tropopause.

As each forward trajectory may cross several receptor regions, we determined the fraction of time the trajectory spent inside each receptor region from the number of 30 min trajectory time steps that were inside the receptor region. An example for this analysis is shown in Fig. 12 for the flight on 13 August 2008. Each panel shows all the forward trajectories (south of the northern cut-off) for this flight in grey. The trajectories which cross the different receptor regions are shown in red (North America), magenta (central Pacific), green (central Africa), blue (the Mediterranean), and orange (South Asian monsoon). The lowermost right panel shows the trajectories, with stratospheric parts in yellow (for thermal tropopause criterion) and pink (dynamical tropopause criterion). As mentioned above, the dynamical tropopause is usually somewhat higher than the thermal tropopause. Therefore the pink trajectories form a subset of the yellow trajectories except for one trajectory which is classified as stratospheric according to the dynamical tropopause but not according to the thermal tropopause.

The aggregate results for the receptor region analysis are shown in Fig. 13. It shows the percentages of trajectories reaching the seven receptor regions defined in Table 2 averaged for each month between June and September 2008. Since a trajectory may reach more than one receptor region (e.g. central Africa and Mediterranean, central Pacific and North America, or dynamical PV stratosphere and thermal TP stratosphere), the totals exceed 100 %. The least receptor region overlap is observed in September, while the trajectories in July reach the largest number of receptor regions. July is also different from the other months in that it has the largest fraction of outflow to the west, i.e. to central Africa (green bar) and further on to the Mediterranean (blue bar). This may be a peculiarity for 15/16 July 2008, when the flights took place. Note that in July there were only two flights and not four as in the other months.

The latitudinal distribution of the receptor regions (not shown) for the air sampled by the CARIBIC aircraft varies from flight to flight, but the general tendency is that air sampled in the north is mostly either exported towards the east or entering the stratosphere, while most air masses that are exported towards Africa and the Mediterranean have been sampled in the southern part of the flight track through the UTAC. Importantly, air sampled in the middle of the UTAC, i.e. at the location of the wind reversal, and a few degrees south appears to have the highest likelihood of being transported to the stratosphere. In September, transport is somewhat different, with less air sampled in the middle of the UTAC moving to the stratosphere, but instead more air remains in the UTAC and the region where air exported towards the east is expanding southwards. This shift in the latitudinal distribution may be the result of a weakening monsoon circulation towards the end of the monsoon season. The actual monsoon withdrawal as diagnosed by the India Meteorological Department, however, started in 2008 at the end of September (IMD, 2009). One should also keep in mind that the monsoon contributes only partially to the air and the pollutants which reach the receptor regions. Especially for receptor regions far away, e.g. North America, the monsoon will only have a limited influence. But in special cases the monsoon may even influence air mass composition as far away as the east coast of Canada (see Supplement Sect. S1 for a case documented by CARIBIC in September 2007).

3.3.2 Estimating transport times

An important cross-check of the FLEXPART trajectory calculations is possible by comparing with the photochemical age of air pollutants estimated from ratios of NMHCs measured in the whole air samples collected during the two flights in July and the first two flights in August 2008. Since sample collection only took place during the first two flight per month, no samples are available for the last two flights in August. The samples from June and September did not give consistent photochemical age estimates. The photochemical age is used as a proxy for the time elapsed since the pollutants had been emitted into the air mass. Details of the NMHC age calculation have been published previously by Baker et al. (2011). For air samples collected south of the wind reversal that had recently been convectively lifted to cruise altitude, we use an estimated mean OH concentration $\langle[OH]\rangle$ of 2.48×10^6 molecules cm^{-3} (Spivakovsky et al., 2000). For samples collected north of the

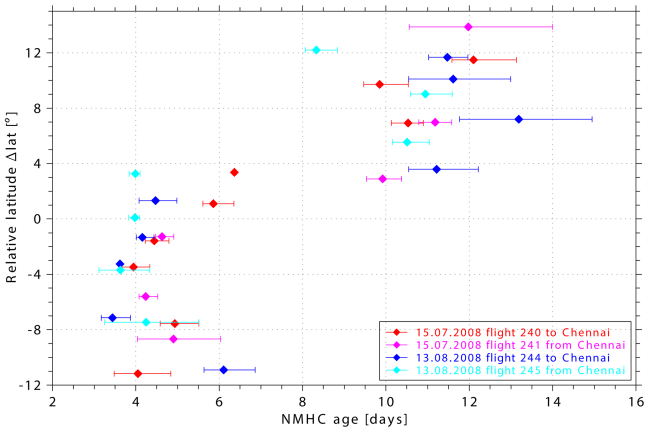

Figure 14. Photochemical age of pollutants in the air samples estimated from NMHC ratios (see Sect. 3.3.2 and Baker et al., 2011) versus relative latitude for the flights in July and the first two flights in August. Note the clustering of the chemically young samples close to and south of the wind reversal ($\Delta\text{lat} < \sim 3°$) and the older more chemically processed samples further north. Shown is the mean chemical age together with the minimum and maximum age determined from the propane/ethane, *n*-butane/ethane, and *n*-butane/propane ratios.

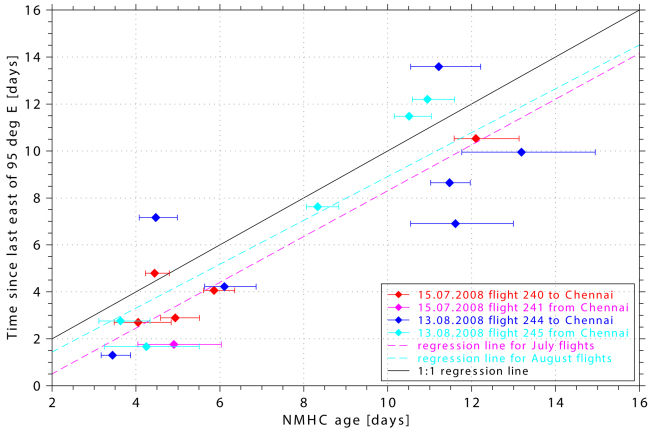

Figure 15. Comparison of the photochemical age of air estimated from NMHC ratios and the time the air had last been east of 95° E according to the FLEXPART trajectory calculations. Shown are the mean chemical age together with the minimum and maximum age determined from the propane / ethane, *n*-butane / ethane, and *n*-butane / propane ratios. The colours indicate different flights (see legend). The black line indicates perfect agreement of both age estimates, while the dashed lines indicate linear least-squares regression lines of transport time and chemical ages derived from the different NMHC ratios (magenta regression lines for July, light blue for August flights).

wind reversal we instead applied an estimated ⟨[OH]⟩ of 1.44×10^6 molecules cm^{-3} (Spivakovsky et al., 2000). Emission ratios of 0.29 and 0.15 for propane/ethane and *n*-butane / ethane, respectively, were assumed. Figure 14 shows a clear clustering of the NMHC ages, with photochemically younger air in the south ($\Delta\text{lat} < \sim 3°$) which had recent contact with fresh emissions and older air in the north, with more aged air having already experienced several days of photochemical processing during transport in the UTAC. The NMHC-based average ages in the two clusters are 4.5 days (south) compared to 11 days (north).

The comparison of the mean chemical age of the air pollutants with the transport times estimated from the FLEXPART trajectory calculations is shown in Fig. 15. For July, the best fit was found when comparing the time since the air had last been east of 95° E. For August, the correlations do not change much for a source region between 85 and 95° E. Table 3 lists the slopes and squared Pearson correlation coefficients R^2 for source regions at 80 to 100° E. For 95° E, the linear least-squares regression lines have slopes of 0.97 ± 0.19 and 0.93 ± 0.20 and squared Pearson correlation coefficients R^2 of 0.87 and 0.68 for the flights in July and August, respectively. Considering that the NMHC age estimates use surface emission ratios based on ground-based data as the starting point for the age calculations and that convection (which is partly parameterised in the FLEXPART model) is most frequent over the Bay of Bengal, a source region east of 90–95° E seems reasonable and fits to the source regions discussed in Sect. 3.2. Although the degree of significance of the correlations is largely due to the existence of two clusters of data, the approximate overall agreement between the two methods provides confidence that our interpretation of pollutant distributions and transport within the UTAC is realistic. In most cases where there is a large disagreement between NMHC chemical age and FLEXPART transport age, the NMHC ages show a large spread. Reasons for this may be mixing with background air, different source ratios than assumed in the analysis, or situations where the OH concentrations deviated from the assumed climatological averages used in the NMHC age calculations. Uncertainties in ⟨[OH]⟩ of ±25 % correspond to uncertainties of the derived NMHC ages of 20–33 % (see Baker et al., 2011).

3.3.3 Monsoon UTAC "leak" rates

The South Asian summer monsoon UTAC is often described as a processing reactor for the pollution emitted at the surface which is rapidly transported upward by convection to become trapped in the UTAC (e.g. Park et al., 2008; Schuck et al., 2010; Randel and Jensen, 2013; Barret et al., 2016, and references therein). However, the horizontal wind fields shown in Fig. 1 and the forward trajectories in Fig. 12 indicate that the trapping is temporary, i.e. the trajectories do not stay in the monsoon UTAC forever. As soon as 6 days after the flight, around 50 % of the trajectories have left the UTAC (see Fig. 16 described below). At the south-western part of the UTAC, air escapes to central Africa, part of which may return via the Mediterranean and the Middle East to become

Table 3. Slopes of the correlation of NMHC photochemical ages and FLEXPART trajectory transport times for different assumed source regions. The squared Pearson correlation coefficients (R^2) are shown in parentheses (see Sect. 3.3.2 for details).

Longitude limit	July	August
80° E	1.12 ± 0.19 (R^2 0.72)	0.91 ± 0.17 (R^2 0.68)
85° E	1.01 ± 0.21 (R^2 0.66)	0.90 ± 0.18 (R^2 0.67)
90° E	1.05 ± 0.25 (R^2 0.63)	0.92 ± 0.18 (R^2 0.69)
95° E	0.97 ± 0.19 (R^2 0.87)	0.93 ± 0.20 (R^2 0.68)
100° E	0.84 ± 0.77 (R^2 0.28)	0.99 ± 0.31 (R^2 0.59)

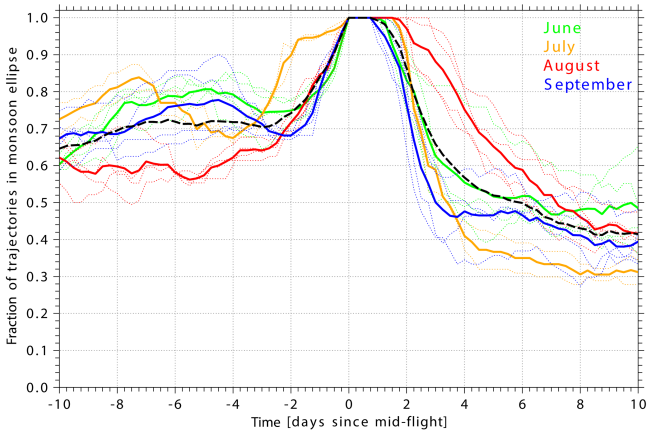

Figure 16. Monsoon leak rates for all flights between June and September 2008. Shown is the fraction of the backward and forward trajectories which started inside the monsoon ellipse ($t = 0$) and are inside the monsoon ellipse at the given time in days before and after the aircraft was inside the monsoon ellipse (see Sect. 3.3.3). The solid coloured lines are monthly means with the results from the single flights indicated by dotted lines. Colours indicate the months. The dashed black line shows the mean leak rate averaged over all flights.

again entrained in the UTAC in the northwest. In the north-eastern region, air is leaving the UTAC with the eastward jet stream and is transported over China towards the Pacific and finally North America. Quantifying these losses is the goal of the leak rate analysis described below.

The calculated trajectories have been used to estimate the residence time of the observed air inside the monsoon ellipse defined above. For this analysis, only the trajectories along the flight track that started inside the ellipse are used. The number of trajectories remaining within the ellipse was determined for the preceding and following 10 days at time steps of 6 h centred around the middle of the time period the flight track spent inside the ellipse, i.e. midway (in time) between when the aircraft entered the monsoon ellipse and when it landed in Chennai and vice versa for southward and northbound flights, respectively. This analysis is similar to the leak rate calculations by Randel and Park (2006, their Fig. 14).

The results, colour-coded for flight month, are shown in Fig. 16. The solid coloured lines show the monthly means, while the dashed black line indicates the average over all months. On average, 65 % of the trajectories had resided inside the monsoon ellipse for at least 10 days, while 30 % of the air had become entrained within the last 3 days prior to measurement. Following the air masses after their measurement shows a different picture: after 6 days only 50 % of the trajectories, on average, had remained within the ellipse. However, while fewer trajectories were within the ellipse before the measurement in August, they tended to remain inside longer after the measurement than in the other months. Especially in June and September, the exit from the ellipse was more rapid than in July and August, related to the weaker monsoon circulation during these months. The calculated leak rates are higher, i.e. the trajectories leave the UTAC region faster, than those calculated by Randel and Park (2006), which is consistent with the much larger monsoon anticyclone area definition used by these authors.

An explanation for the asymmetric shape of the calculated leak rates is related to the position of the aircraft within the UTAC and hence within the monsoon ellipse defined above. The flight tracks cross the western part of the ellipse. The UTAC has two main points of air discharge: one in the southwest, where air is transported westwards towards Africa, and one in the north-east, where it is transported eastwards towards China and the Pacific Ocean. In the northern part of our flight track inside the UTAC, the air masses observed had not left towards Africa but stayed inside the UTAC. In the forward direction, the air masses have a chance of leaving the UTAC at its north-eastern part, i.e. towards China and the Pacific Ocean. Having traversed to the southern part, the air masses observed have not left towards the Pacific but stayed inside the UTAC. But looking forward again, the air masses have a chance of leaving the UTAC towards Africa. Since the calculated leak rates are an average over all trajectories started inside the UTAC, it is consistent with our understanding of the monsoon circulation that looking backwards, there is a tendency that the air masses have already been for quite some time inside the UTAC (at least the majority of the trajectories) while looking forwards, the air masses have a higher chance of leaving the UTAC quickly (or at least faster than they have entered the UTAC). In August, which

from all CARIBIC data seems to be the most representative monsoon month (red lines in Fig. 16), the UTAC contains the air masses more strongly than in the other months. In addition, Figs. S30 and S31 in the Supplement show that the trapping efficiency changes little even when considering altitudes 2 km above the actual flight level. This is somewhat unexpected. As the UTAC has its maximum some kilometres above the actual flight altitude of the CARIBIC aircraft of $\sim$ 11–12 km (Park et al., 2008), a stronger confinement at altitudes above the CARIBIC flight altitudes is expected.

4 Conclusions

The data from the CARIBIC passenger aircraft observatory discussed in this study cover the South Asian summer monsoon season 2008 from June to September. Even though the flights crossed the western part of the monsoon UTAC and not its centre and the cruise altitude of $\sim$ 11 km is at the lower boundary of the UTAC (e.g. Park et al., 2008), Figs. 6 and 7 show systematic profiles and trace gas correlations over a distance of 3500 km (approximately from Teheran, Iran, to Chennai, India), as previously reported by Schuck et al. (2010) and Baker et al. (2011). This matches earlier observations from CARIBIC phase 1 during flights from Germany to Colombo, Sri Lanka, and Malé, Maldives (not shown), in the summers 1998–2000, despite consisting of a more limited chemical data set (Hermann et al., 2003; Zahn et al., 2002, and unpublished data).

In accordance with our current understanding of the South Asian summer monsoon and in particular its role trapping surface air that was rapidly transported upwards by convective activity, all the CARIBIC observations during the monsoon months in this region, although they were made in different years, fit the same overall picture of pollution build-up in the UTAC. Starting from this consistent data set, of particular interest is, on the one hand, the understanding of the chemical composition of the air in the UTAC and, on the other hand, the export of this air to other regions, for which the CARIBIC flight to Toronto in September 2007 (see Sect. S1 in the Supplement) gives a good example.

Based on the measured reversal of the zonal wind at flight altitude across the centre of the UTAC located at 27° N in June to 23° N in September (Table 1, cf. New Delhi 28.4° N, Calcutta 22.3° N), the chemical and aerosol particle data are presented using relative latitude with respect to the wind reversal and by doing so provide a very consistent picture of humid, recently polluted, low-O_3, medium-CO air and low-NO_y air with a high burden of aerosol particles in the south and a strengthening tendency (increasing CO and O_3, declining humidity) towards the centre of the UTAC. Northwards from there dry air is observed, with higher NO_y but strongly declining CO, moderately declining O_3 (up to a relative latitude Δlat of around 12°), and low aerosol particle number concentrations.

The vertical profiles of O_3 and CO over Chennai are very distinct compared to other profile observations over India (Sheel et al., 2014; Sahu et al. 2014). They are likely influenced by the local emissions in the Chennai area together with the advection of clean maritime air and polluted air from other parts of India and the surrounding region to form the characteristic "C shape" observed for CO in all months except July. In that month a strong free-tropospheric CO enhancement of up to 116 ppb was observed, which cannot be explained solely by local convection of polluted surface air but is instead probably due to long-range transport of polluted air masses. Detailed modelling studies with the WRF-Chem online regional chemistry transport model to understand these vertical profiles have been published separately (Ojha et al., 2016).

Hydrocarbon ratios used in photochemical age of air calculations show that the air masses in the southern part of the UTAC are younger (chemical ages between 3.5 and 6.5 days) than in the north (chemical ages between 10 and 13.5 days). The clustering of the chemical ages compares well with that based on the transport age determined from the FLEXPART backward trajectories, namely 1–7 days compared to 7–14 days for transport from 95° E to the CARIBIC flight track. The spread in the FLEXPART transport ages is larger and they are in general higher by 0.5–1.5 days. Given the uncertainties of air mass trajectory calculations, the problems in how to determine its starting point in time over polluting sources, and the uncertainty in photochemical age that may be affected by dilution with background air, the correspondence is encouraging.

Air sampled by CARIBIC originated from a large region. Although the convection over the Bay of Bengal is greatest, for a quantification of its effect on pollution the vertical transport has to be combined with the emission source distributions, which is beyond the scope of this study. For the vertical profiles, such a study has been done by Ojha et al. (2016). Instead, we have focused on the FLEXPART backward-trajectory-based footprint (air at cruise level that had come from below 5 km) for air in the southern and northern part of the UTAC. For the southern part, the footprint is situated somewhat more to the south and west. For August the surface area of the footprint is largest (see Figs. S26–S29 in the Supplement). When the UTAC wanes in September, and its centre moves south to reach 23° N north, the footprint likewise shifts southward and is more concentrated over the Indian subcontinent than in the other months. However, no major differences in footprint for air in the southern compared to the northern part of the UTAC exist; the age difference seems to be the fundamental difference. In other words, the difference between the two regimes is due to the time elapsed since fresh pollution was injected into the UTAC.

The receptor region analyses and the "leak" rates show that air in the southern part of the UTAC is mostly in an ozone-forming chemical regime (Fig. 7) and part of it is exported towards central Africa and the Mediterranean. In contrast,

the air in the northern part, which features an ozone neutral or partially even ozone destroying chemical regime, is exported towards China and the Pacific Ocean and in rare cases even up to the east coast of North America (Sect. S1 in the Supplement). Export from the UTAC into the stratosphere peaked in June and July (Fig. 13). With CO values declining from June onward, this implies an "optimal" input of CO into the lowermost stratosphere. However, approximately two-thirds of the air is dispersed within the troposphere. Such transport to the stratosphere has been observed in a similar way by the German HALO (High Altitude and LOng range) research aircraft, which detected monsoon pollution transported to the lowermost stratosphere over Europe in late summer 2012 during the TACTS (Transport And Composition in the upper troposphere/lowermost stratosphere) campaign (A. Roiger, private communication, 2014).

The large-scale movement in the UTAC as in a large-scale atmospheric "merry-go-round" is not without losses (Fig. 16). While surface air very high in pollutants reaches the UTAC from below and becomes trapped, similar amounts of air leak out of the system, mostly at its northeastern and southwestern edges. Still, the trapping process is impressive. Even going back in time 10 days prior to sampling by CARIBIC, on average 65 % of the back trajectories had resided within the UTAC defined for this calculation as an ellipse. After having been probed by CARIBIC, only 40 % of the trajectories stay in the UTAC ellipse for more than 10 days. This asymmetry is an artifact of the geographical skew in the sampling by CARIBIC. Interestingly, calculations show that the leakage rates 2 km above cruise altitude of CARIBIC are not significantly lower (Sect. S8 in the Supplement). A mass balance of the UTAC is beyond the scope of this work. Undoubtedly, air from outside the UTAC is also being entrained, leading to dilution that intensifies towards its borders.

The population of the monsoon source region of South Asia was about 1.4 billion people in 2008 and the population is still growing. Together with the economic development in this region, this means that the pollutant emissions today are larger than in 2008 and will further increase in the future. This also encompasses export of even more polluted air as shown in this study with implications for the atmospheric chemistry and air quality in the receiving regions.

The Supplement related to this article is available online at doi:10.5194/acp-16-3609-2016-supplement.

Acknowledgements. We wish to thank all CARIBIC partners as well as Lufthansa, especially T. Dauer and A. Waibel, and Lufthansa Technik for their ongoing support for many years. We especially acknowledge D. Scharffe, C. Koeppel, and S. Weber for the operation of this complex platform. The FLEXPART model was provided by A. Stohl at the Norwegian Institute for Air Research (NILU) and was used with meteorological data from the European Centre for Medium-Range Weather Forecasts (ECMWF).

The article processing charges for this open-access publication were covered by the Max Planck Society.

Edited by: E. Harris

References

Assonov, S. S., Brenninkmeijer, C. A. M., Schuck, T. J., and Taylor, P.: Analysis of ^{13}C and ^{18}O isotope data of CO_2 in CARIBIC aircraft samples as tracers of upper troposphere/lower stratosphere mixing and the global carbon cycle, Atmos. Chem. Phys., 10, 8575–8599, doi:10.5194/acp-10-8575-2010, 2010.

Baker, A. K., Slemr, F., and Brenninkmeijer, C. A. M.: Analysis of non-methane hydrocarbons in air samples collected aboard the CARIBIC passenger aircraft, Atmos. Meas. Tech., 3, 311–321, doi:10.5194/amt-3-311-2010, 2010.

Baker, A. K., Schuck, T. J., Slemr, F., van Velthoven, P., Zahn, A., and Brenninkmeijer, C. A. M.: Characterization of non-methane hydrocarbons in Asian summer monsoon outflow observed by the CARIBIC aircraft, Atmos. Chem. Phys., 11, 503–518, doi:10.5194/acp-11-503-2011, 2011.

Baker, A. K., Schuck, T. J., Brenninkmeijer, C. A. M., Rauthe-Schöch, A., Slemr, F., van Velthoven, P. F. J., and Lelieveld, J.: Estimating the contribution of monsoon-related biogenic production to methane emissions from South Asia using CARIBIC observations, Geophys. Res. Lett., 10, L10813, doi:10.1029/2012GL051756, 2012.

Barret, B., Sauvage, B., Bennouna, Y., and Le Flochmoen, E.: Upper tropospheric CO and O3 budget during the Asian Summer Monsoon, Atmos. Chem. Phys. Discuss., doi:10.5194/acp-2015-1011, in review, 2016.

Brenninkmeijer, C. A. M., Crutzen, P., Boumard, F., Dauer, T., Dix, B., Ebinghaus, R., Filippi, D., Fischer, H., Franke, H., Frieß, U., Heintzenberg, J., Helleis, F., Hermann, M., Kock, H. H., Koeppel, C., Lelieveld, J., Leuenberger, M., Martinsson, B. G., Miemczyk, S., Moret, H. P., Nguyen, H. N., Nyfeler, P., Oram, D., O'Sullivan, D., Penkett, S., Platt, U., Pupek, M., Ramonet, M., Randa, B., Reichelt, M., Rhee, T. S., Rohwer, J., Rosenfeld, K., Scharffe, D., Schlager, H., Schumann, U., Slemr, F., Sprung, D., Stock, P., Thaler, R., Valentino, F., van Velthoven, P., Waibel, A., Wandel, A., Waschitschek, K., Wiedensohler, A., Xueref-Remy, I., Zahn, A., Zech, U., and Ziereis, H.: Civil aircraft for the regular investigation of the atmosphere based on an instrumented container: The new CARIBIC system, Atmos. Chem. Phys., 7, 4953–4976, doi:10.5194/acp-7-4953-2007, 2007.

Brough, N., Reeves, C. E., Penkett, S. A., Stewart, D. J., Dewey, K., Kent, J., Barjat, H., Monks, P. S., Ziereis, H., Stock, P., Huntrieser, H., and Schlager, H.: Intercomparison of aircraft instruments on board the C-130 and Falcon 20 over southern Germany during EXPORT 2000, Atmos. Chem. Phys., 3, 2127–2138, doi:10.5194/acp-3-2127-2003, 2003.

Chakraborty, A., Nanjundiah, R. S., and Srinivasan, J.: Impact of African orography and the Indian summer monsoon

on the low-level Somali jet, Int. J. Climatol., 29, 983–992, doi:10.1002/joc.1720, 2009.

Chen, B., Xu, X. D., Yang, S., and Zhao, T. L.: Climatological perspectives of air transport from atmospheric boundary layer to tropopause layer over Asian monsoon regions during boreal summer inferred from Lagrangian approach, Atmos. Chem. Phys., 12, 5827–5839, doi:10.5194/acp-12-5827-2012, 2012.

Crawford, J. and Pan, L.: Atmospheric composition and the Asian monsoon: Results from a side meeting at the 12th IGAC Science Conference in Beijing, 17–21 September 2012, SPARC Newsletter, 40, p. 67, 2013.

Devasthale, A. and Fueglistaler, S.: A climatological perspective of deep convection penetrating the TTL during the Indian summer monsoon from the AVHRR and MODIS instruments, Atmos. Chem. Phys., 10, 4573–4582, doi:10.5194/acp-10-4573-2010, 2010.

Dyroff, C., Zahn, A., Christner, E., Forbes, R., Tompkins, A. M., and van Velthoven, P. F. J.: Comparison of ECMWF analysis and forecast humidity data to CARIBIC upper troposphere and lower stratosphere observations, Q. J. Roy. Meteor. Soc., 141, 833–844, doi:10.1002/qj.2400, 2015.

Fairlie, T. D., Vernier, J.-P., Natarajan, M., and Bedka, K. M.: Dispersion of the Nabro volcanic plume and its relation to the Asian summer monsoon, Atmos. Chem. Phys., 14, 7045–7057, doi:10.5194/acp-14-7045-2014, 2014.

Fishman, J. and Crutzen, P. J.: The origin of ozone in the troposphere, Nature, 274, 855–858, doi:10.1038/274855a0, 1978.

Garny, H. and Randel, W. J.: Dynamic variability of the Asian monsoon anticyclone observed in potential vorticity and correlations with tracer distributions, J. Geophys. Res., 118, 13421–13433, doi:10.1002/2013JD020908, 2013.

Hermann, M. and Wiedensohler, A.: Counting efficiency of condensation particle counters at low-pressures with illustrative data from the upper troposphere, J. Aerosol Sci., 32, 975–991, doi:10.1016/S0021-8502(01)00037-4, 2001.

Hermann, M., Heintzenberg, J., Wiedensohler, A., Zahn, A., Heinrich, G., and Brenninkmeijer, C. A. M.: Meridional distributions of aerosol particle number concentrations in the upper troposphere and lower stratosphere obtained by Civil Aircraft for Regular Investigation of the Atmosphere Based on an Instrument Container (CARIBIC) flights, J. Geophys. Res., 108, 4114, doi:10.1029/2001JD001077, 2003.

India Meteorological Department (IMD): Annual Report 2008, available at: http://metnet.imd.gov.in/imdnews/ar2008.pdf (last access: 19 February 2016), 2009.

Kar, J., Bremer, H., Drummond, J. R., Rochon, Y. J., Jones, D. B. A., Nichitiu, F., Zou, J., Liu, J., Gille, J. C., Edwards, D. P., Deeter, M. N., Francis, G., Ziskin, D., and Warner, J.: Evidence of vertical transport of carbon monoxide from Measurements of Pollution in the Troposphere (MOPITT), Geophys. Res. Lett., 31, L23105, doi:10.1029/2004GL021128, 2004.

Kurokawa, J., Ohara, T., Morikawa, T., Hanayama, S., Janssens-Maenhout, G., Fukui, T., Kawashima, K., and Akimoto, H.: Emissions of air pollutants and greenhouse gases over Asian regions during 2000–2008: Regional Emission inventory in ASia (REAS) version 2, Atmos. Chem. Phys., 13, 11019–11058, 10.5194/acp-13-11019-2013, 2013.

Lawrence, M. G. and Lelieveld, J.: Atmospheric pollutant outflow from southern Asia: a review, Atmos. Chem. Phys., 10, 11017–11096, doi:10.5194/acp-10-11017-2010, 2010.

Lelieveld, J., Berresheim, H., Borrmann, S., Crutzen, P. J., Dentener, F. J., Fischer, H., Feichter, J., Flatau, P. J., Heland, J., Holzinger, R., Korrmann, R., Lawrence, M. G., Levin, Z., Markowicz, K. M., Mihalopoulos, N., Minikin, A., Ramanathan, V., de Reus, M., Roelofs, G. J., Scheeren, H. A., Sciare, J., Schlager, H., Schultz, M., Siegmund, P., Steil, B., Stephanou, E. G., Stier, P., Traub, M., Warneke, C., Williams, J., and Ziereis, H.: Global air pollution crossroads over the Mediterranean, Science, 298, 794–799, doi:10.1126/science.1075457, 2002.

Lelieveld, J., Brühl, C., Jöckel, P., Steil, B., Crutzen, P. J., Fischer, H., Giorgetta, M. A., Hoor, P., Lawrence, M. G., Sausen, R., and Tost, H.: Stratospheric dryness: model simulations and satellite observations, Atmos. Chem. Phys., 7, 1313–1332, doi:10.5194/acp-7-1313-2007, 2007.

Li, Q., Jacob, D. J., Logan, J. A., Bey, I., Yantosca, R. M., Liu, H., Martin, R. V., Fiore, A. M., Field, B. D., Duncan, B. N., and Thouret, V.: A tropospheric ozone maximum over the Middle East, Geophys. Res. Lett., 28, 3235–3238, doi:10.1029/2001GL013134, 2001.

Liang, Q., Jaeglé, L., Hudman, R. C., Turquety, S., Jacob, D. J., Avery, M. A., Browell, E. V., Sachse, G. W., Blake, D. R., Brune, W., Ren, X., Cohen, R. C., Dibb, J. E., Fried, A., Fuelberg, H., Porter, M., Heikes, B. G., Huey, G., Singh, H. B., and Wennberg, P. O.: Summertime influence of Asian pollution in the free troposphere over North America, J. Geophys. Res., 112, D12S11, doi:10.1029/2006JD007919, 2007.

Liu, H., Jacob, D. J., Bey, I., Yantosca, R., Duncan, B. N., and Sachse, G. W.: Transport pathways for Asian pollution outflow over the Pacific: interannual and seasonal variations, J. Geophys. Res., 108, 8786, doi:10.1029/2002JD003102, 2003.

Liu, J. J., Jones, D. B. A., Worden, J. R., Noone, D., Parrington, M., and Kar, J.: Analysis of the summertime buildup of tropospheric ozone abundances over the Middle East and North Africa as observed by the Tropospheric Emission Spectrometer instrument, J. Geophys. Res., 114, D05304, doi:10.1029/2008JD010993, 2009.

Ojha, N., Pozzer, A., Rauthe-Schöch, A., Baker, A. K., Yoon, J., Brenninkmeijer, C. A. M., and Lelieveld, J.: Ozone and carbon monoxide over India during the summer monsoon: regional emissions and transport, Atmos. Chem. Phys., 16, 3013–3032, doi:10.5194/acp-16-3013-2016, 2016.

O'Sullivan, D. A.: Temporal and spatial variability of halogenated compounds and other trace gases, Ph.D. thesis, University of East Anglia, Norwich, UK, 2007.

Pan, L., Crawford, J., Tanimoto, H., Lawrence, M., Panday, A., Babu, S. S., Barret, B., Schlager, H., Konopka, P., and Bian, J.: Report on the Atmospheric Composition and the summer Asian Monsoon (ACAM) workshop, 9–12 June 2013, Kathmandu, Nepal, SPARC Newsletter, 42, 40–45, 2014.

Park, M., Randel, W. J., Emmons, L. K., Bernath, P. F., Walker, K. A., and Boone, C. D.: Chemical isolation in the Asian monsoon anticyclone observed in Atmospheric Chemistry Experiment (ACE-FTS) data, Atmos. Chem. Phys., 8, 757–764, doi:10.5194/acp-8-757-2008, 2008.

Parrish, D. D., Holloway, J. S., Trainer, M., Murphy, P. C., Fehsenfeld, F. C., and Forbes, G. L.: Export of North American ozone

pollution to the North Atlantic ocean, Science, 259, 1436–1439, doi:10.1126/science.259.5100.1436, 1993.

Parrish, D. D., Trainer, M., Holloway, J. S., Yee, J. E., Warshawsky, M. S., Fehsenfeld, F. C., Forbes, G. L., and Moody, J. L.: Relationships between ozone and carbon monoxide at surface sites in the North Atlantic region, J. Geophys. Res., 103, 13357–13376, doi:10.1029/98JD00376, 1998.

Patra, P. K., Niwa, Y., Schuck, T. J., Brenninkmeijer, C. A. M., Machida, T., Matsueda, H., and Sawa, Y.: Carbon balance of South Asia constrained by passenger aircraft CO_2 measurements, Atmos. Chem. Phys., 11, 4163–4175, doi:10.5194/acp-11-4163-2011, 2011.

Randel, W. J. and Jensen, E. J.: Physical processes in the tropical tropopause layer and their roles in a changing climate, Nature Geosci., 6, 169–176, doi:10.1038/ngeo1733, 2013.

Randel, W. J. and Park, M.: Deep convective influence on the Asian summer monsoon anticyclone and associated tracer variability observed with Atmospheric Infrared Sounder (AIRS), J. Geophys. Res., 111, D12314, doi:10.1029/2005JD006490, 2006.

Randel, W. J., Park, M., Emmons, L., Kinnison, D., Bernath, P., Walker, K. A., Boone, C., and Pumphrey, H.: Asian monsoon transport of pollution to the stratosphere, Science, 328, 611–613, doi:10.1126/science.1182274, 2010.

Sahu, L. K., Lal, S., Thouret, V., and Smit, H. G.: Climatology of tropospheric ozone and water vapour over Chennai: a study based on MOZAIC measurements over India, Int. J. Climatol., 31, 920–936, doi:10.1002/joc.2128, 2011.

Sahu, L. K., Sheel, V., Kajino, M., Deushi, M., Gunthe, S. S., Sinha, P. R., Sauvage, B., Thouret, V., and Smit, H. G.: Seasonal and interannual variability of tropospheric ozone over an urban site in India: a study based on MOZAIC and CCM vertical profiles over Hyderabad, J. Geophys. Res., 119, 3615–3641, doi:10.1002/2013JD021215, 2014.

Scharffe, D., Slemr, F., Brenninkmeier, C. A. M., and Zahn, A.: Carbon monoxide measurements onboard the CARIBIC passenger aircraft using UV resonance fluorescence, Atmos. Meas. Tech., 5, 1753–1760, doi:10.5194/amt-5-1753-2012, 2012.

Scheeren, H. A., Lelieveld, J., Roelofs, G. J., Williams, J., Fischer, H., de Reus, M., de Gouw, J. A., C.Warneke, Holzinger, R., Schlager, H., Klüpfel, T., Bolder, M., van der Veen, C., and Lawrence, M.: The impact of monsoon outflow from India and Southeast Asia in the upper troposphere over the eastern Mediterranean, Atmos. Chem. Phys., 3, 1589–1608, doi:10.5194/acp-3-1589-2003, 2003.

Schuck, T. J., Brenninkmeijer, C. A. M., Slemr, F., Xueref-Remy, I., and Zahn, A.: Greenhouse gas analysis of air samples collected onboard the CARIBIC passenger aircraft, Atmos. Meas. Tech., 2, 449–464, doi:10.5194/amt-2-449-2009, 2009.

Schuck, T. J., Brenninkmeijer, C. A. M., Baker, A. K., Slemr, F., van Velthoven, P. F. J., and Zahn, A.: Greenhouse gas relationships in the Indian summer monsoon plume measured by the CARIBIC passenger aircraft, Atmos. Chem. Phys., 10, 3965–3984, doi:10.5194/acp-10-3965-2010, 2010.

Sheel, V., Sahu, L. K., Kajino, M., Deushi, M., Stein, O., and Nedelec, P.: Seasonal and interannual variability of carbon monoxide based on MOZAIC observations, MACC reanalysis, and model simulations over an urban site in India, J. Geophys. Res., 119, 9123–9141, doi:10.1002/2013JD021425, 2014.

Spivakovsky, C. M., Logan, J. A., Montzka, S. A., Balkanski, Y. J., Foreman-Fowler, M., Jones, D. B. A., Horowitz, L. W., Fusco, A. C., Brenninkmeijer, C. A. M., Prather, M. J., Wofsy, S. C., and McElroy, M. B.: Three-dimensional climatological distribution of tropospheric OH: update and evaluation, J. Geophys. Res., 105, 8931–8980, doi:10.1029/1999JD901006, 2000.

Stohl, A., Forster, C., Frank, A., Seibert, P., and Wotawa, G.: Technical note: The Lagrangian particle dispersion model FLEXPART version 6.2, Atmos. Chem. Phys., 5, 2461–2474, doi:10.5194/acp-5-2461-2005, 2005.

Stohl, A., Sodemann, H., Eckhardt, S., Frank, A., Seibert, P., and Wotawa, G.: The Lagrangian particle dispersion model FLEXPART version 8.2, Tech. rep., Norwegian Institute of Air Research (NILU), Kjeller, Norway, available at: http://flexpart.eu/, last access: 19 February 2016, 2010.

Trainer, M., Parrish, D. D., Goldan, P. D., Roberts, J., and Fehsenfeld, F. C.: Review of observation-based analysis of the regional factors influencing ozone concentrations, Atmos. Environ., 34, 2045–2061, doi:10.1016/S1352-2310(99)00459-8, 2000.

Traub, M. and Lelieveld, J.: Cross-tropopause transport over the eastern Mediterranean, J. Geophys. Res., 108, 4712, doi:10.1029/2003JD003754, 2003.

Umezawa, T., Baker, A. K., Oram, D., Sauvage, C., O'Sullivan, D., Rauthe-Schöch, A., Montzka, S. A., Zahn, A., and Brenninkmeijer, C. A. M.: Methyl chloride in the upper troposphere observed by the CARIBIC passenger aircraft observatory: large-scale distributions and Asian summer monsoon outflow, J. Geophys. Res., 119, 5542–5558, doi:10.1002/2013JD021396, 2014.

Umezawa, T., Baker, A. K., Brenninkmeijer, C. A. M., Zahn, A., Oram, D. E., and van Velthoven, P. F. J.: Methyl chloride as a tracer of tropical tropospheric air in the lowermost stratosphere inferred from IAGOS-CARIBIC passenger aircraft measurements, J. Geophys. Res., 120, 12313–12326, doi:10.1002/2015JD023729, 2015.

Vogel, B., Günther, G., Müller, R., Grooß, J.-U., and Riese, M.: Impact of different Asian source regions on the composition of the Asian monsoon anticyclone and of the extratropical lowermost stratosphere, Atmos. Chem. Phys., 15, 13699–13716, doi:10.5194/acp-15-13699-2015, 2015.

Voulgarakis, A., Telford, P. J., Aghedo, A. M., Braesicke, P., Faluvegi, G., Abraham, N. L., Bowman, K. W., Pyle, J. A., and Shindell, D. T.: Global multi-year O_3–CO correlation patterns from models and TES satellite observations, Atmos. Chem. Phys., 11, 5819–5838, doi:10.5194/acp-11-5819-2011, 2011.

Weigelt, A., Hermann, M., van Velthoven, P. F. J., Brenninkmeijer, C. A. M., Schlaf, G., Zahn, A., and Wiedensohler, A.: Influence of clouds on aerosol particle number concentrations in the upper troposphere, J. Geophys. Res., 114, D01204, doi:10.1029/2008JD009805, 2009.

Xiong, X., Houweling, S., Wei, J., Maddy, E., Sun, F., and Barnet, C.: Methane plume over south Asia during the monsoon season: Satellite observation and model simulation, Atmos. Chem. Phys., 9, 783–794, doi:10.5194/acp-9-783-2009, 2009.

Zahn, A., Brenninkmeijer, C. A. M., Asman, W. A. H., Crutzen, P. J., Heinrich, G., Fischer, H., Cuijpers, J. W. M., and van Velthoven, P. F. J.: Budgets of O_3 and CO in the upper troposphere: CARIBIC passenger aircraft results 1997–2001, J. Geophys. Res., 107, 4337, doi:10.1029/2001JD001529, 2002.

Zahn, A., Weppner, J., Widmann, H., Schlote-Holubek, K., Burger, B., Kühner, T., and Franke, H.: A fast and precise chemiluminescence ozone detector for eddy flux and airborne application, Atmos. Meas. Tech., 5, 363–375, doi:10.5194/amt-5-363-2012, 2012.

Zahn, A., Christner, E., van Velthoven, P. F. J., Rauthe-Schöch, A., and Brenninkmeijer, C. A. M.: Processes controlling water vapor in the upper troposphere / lowermost stratosphere: An analysis of eight years of monthly measurements by the IAGOS-CARIBIC observatory, J. Geophys. Res., 119, 11505–11525, doi:10.1002/2014JD021687, 2014.

Ziereis, H., Schlager, H., Schulte, P., van Velthoven, P. F. J., and Slemr, F.: Distributions of NO, NO_x, and NO_y in the upper troposphere and lower stratosphere between 28° and 61° N during POLINAT 2, J. Geophys. Res., 105, 3653–3664, doi:10.1029/1999JD900870, 2000.